A Laboratory Study on the Effect of Helmet Fit on Biomechanical Measures of Head and Neck Injury in Simulated Impact

by

Henry Y. Yu

A thesis submitted in partial fulfillment of the requirements for the degree of

Master of Science

Department of Mechanical Engineering
University of Alberta

ABSTRACT

Conventional wisdom and the language in international helmet testing and certification standards suggest that appropriate helmet fit and retention during an impact are important factors in protecting the helmet wearer from impact-induced injury. This thesis aims to investigate impact-induced injury mechanisms in different helmet fit scenarios through analysis of simulated helmeted impacts with an anthropometric test device (ATD), an array of headform acceleration transducers and neck force/moment transducers, a dual high speed camera system, and helmet-fit force sensors developed in our research group based on Bragg gratings in optical fibre. To quantify fit and track dynamic helmet movement, novel methods were developed using fit force sensors and high speed cameras respectively. The development of these methods are described in this thesis. The application of these tools and existing practices are implemented in simulated helmet impacts.

To simulate impacts, an instrumented headform and flexible neck fall along a linear guide rail onto an anvil. An instrumented Hybrid III headform and neck is fit with a crash helmet and several fit scenarios can be simulated by making context specific adjustments to the helmet position index and/or helmet size. Specifically, 4 fit scenarios were studied: a normal, oversized, forward, and backward fit. Impact condition simulate a variety of scenarios, including a low (4 m/s) and high (6 m/s) impact velocity, a flat and angled anvil, as well as head and torso-first impacts. To quantify helmet retention, the movement of the helmet on the head is quantified using post-hoc image analysis. To quantify head and neck injury potential, biomechanical measures based on headform acceleration and neck force/moment are measured. These biomechanical measures, through comparison with established human tolerance curves, can estimate risk of severe life threatening and/or mild diffuse brain injury and osteoligamentous neck injury. Poor helmet fit did not significantly increase risk of skull

fracture based on measured linear head acceleration. A backward fit was shown to increase the likelihood of brain injuries in certain torso-first impacts. Neck injury was found to be consistent between fit conditions in all tested impact scenarios. Helmet movement was found to be greatest in the backward fit scenario, with the greatest helmet displacements observed in torso first impacts indicating that in torso impacts more of the head could be exposed for subsequent impacts following a first impact.

In summary, helmets remained effective in mitigating risk of head and neck injury indicating that as long as the helmet is retained on the head during the first impact, it is an effective protection device. Poor fit did affect helmet retention, suggesting that poor fit in some cases could lead to head exposure and increased likelihood of injury in a second subsequent impact. The results in this thesis document trends in biomechanical measures from a laboratory study with several limitations. These results should not be construed to indicate deficiency in the design of the helmets used.

ACKNOWLEDGEMENTS

TABLE OF CONTENTS

LIST OF TABLES

LIST OF FIGURES

CHAPTER 1

INTRODUCTION

This chapter details the problem of poor helmet fit, why its effects on head and neck injury should be investigated, and how it was investigated.

1.1 Motivation

Traumatic Brain Injury (TBI) is a major worldwide health problem with physical, cognitive, behavioral, or even emotional consequences. It is an injury to the brain caused by principal mechanisms such as falls, assaults, motor-vehicle crashes, or sports-related impacts and has potential outcomes including permanent disability and even death. TBI can cause disruptions to the normal function of the brain, hindering an indivual's ability to live a full and productive life. It is estimated that every year, at least 10 million TBIs are serious enough to result in death or hospitalization [1]. In 2013, the United States Centers for Disease Control and Prevention found that approximately 2.8 million TBI related emergency department visits, hospitalizations, and deaths occurred [2]. About 30% of all injury-related deaths were attributed to TBIs [2]. However, these numbers do not account for cases where a patient is treated for TBI in other settings. These numbers may be further unrepresentative in sports-related TBIs where injuries go unrecognized and thus uncounted. Even mild TBI such as concussion can cause disruptions in an individual's behavior and ability to

perform daily activities. TBIs have also been associated with increased risk of post-injury brain disorders such as depression, epilepsy, and Alzheimer's [1]. To minimize the consequences of TBI of all severity, prevention is crucial. Improving protection against these injuries can be realized through understanding the associated etiology including the mechanical factors leading to impact induced mild brain injury.

Epidemiological evidence suggests that bicycle helmets are effective in protecting against head injuries for cyclists, [3] with a consistent theme presented in biomechanical research [4]. Relative to an unprotected head, a helmeted head sustains relatively less severe head and brain injuries in an impact. However, epidemiological evidence also suggests that relative to a properly fit helmet, poor helmet fit may be associated with increased likelihood of head injury [5, 6, 7]. Depending on the criteria used for proper helmet fit, proper helmet use was found to range between 46% and 100% [7]. Although epidemiology suggests that neck injury in cycling may be uncommon, neck injuries tend to be associated with more severe head impacts and hospitalization [8, 9]. Evidence on whether or not helmet use affects neck injury is mixed [8] and cited epidemiological studies also do not quantify aspects of helmet fit. Despite potentially high rates of improper helmet use and epidemiological evidence suggesting the association between helmet fit and injury likelihood, few biomechanical studies have been performed to assess whether or not correct helmet fit has a significant effect on measures of injury risk. Biomechanists can study the mechanics during an impact to assess probability and severity of head and neck injury.

Part of the issue with poor helmet fit prevalence is associated with the subjective and nonspecific definition of a well fit helmet. A good helmet fit is briefly described in various standards and can generally be characterized by position and stability [10, 11]. A properly fit helmet should sufficiently cover the head, without excessively exposing an individual's forehead or covering an individual's eyes. However, measures of quantifying helmet fit are not regularly used to distinguish different levels of helmet

fit. Methods and metrics for objectively comparing helmet fit do exist in academic literature, and compare factors such as forces between a head and helmet, and head and helmet geometry [12, 13]. Helmet standards do evaluate a helmet's stability and retention, but are incomplete in evaluating helmet stability during impact. Even in academia, no method exists to characterize dynamic helmet stability in impact. Because the importance of stability is synonymous with the helmet's ability to stay on the head and protect from injury, the ability to dynamically gauge helmet stability on the head is invaluable. This understanding could be determined by evaluating helmet movement during impact.

Better understanding of the mechanics of helmet retention and its effects on biomechanical parameters assessing likelihood of injury could lead to unambiguous conclusions concerning the importance of helmet fit. Furthermore, methods for quantifying fit and evaluating helmet stability could provide new tools for assessing helmet performance.

1.2   Problem Statement

The objective of this research is to understand how injury likelihood is affected by different helmet fit scenarios through simulated impacts. With an instrumented anthropometric test device and high-speed videography, impact-induced injury mechanics are investigated. Specifically, the study will investigate helmet fit with varying helmet sizing and positioning scenarios arranged prior to impact. These different fit scenarios will then be subjected to various impact scenarios to completely investigate potential effects of helmet fit. In order to evaluate injury likelihood, kinematic head metrics, kinetic neck loads, and helmet movement will be analyzed to assess the likelihood of head and neck injury compared to a regular fit scenario.

1.3 Thesis Organization

The primary focus of this thesis is to investigate the effect of helmet fit in injury like-
lihood. In order to fully investigate the effects of helmet fit in injury likelihood, new
tools were developed to quantify helmet fit and track helmet movement. This thesis
begins with the development and evaluation of these new methods. A new technique
of measuring fit forces with fibre bragg grating (FBG) optical sensors is discussed and
demonstrated between different fit scenarios. In addition, a new technique of tracking
motion of a helmet relative to a head with two high speed cameras is also discussed.

Subsequently, these tools were employed in a study evaluating the role of helmet
fit in simulated impacts. In addition to the newly developed tools, established biome-
chanical measures are used to assess likelihood of head injury and neck injury. In
this study, the injury likelihood in various helmet fit scenarios will be compared in
different impact scenarios with various biomechanical measures. A verdict concerning
the importance of helmet fit may then be reached.

Aspects of this thesis describing development of experimental methods are pre-
sented in peer reviewed journal publication:

Henry Y. Yu, Brooklynn M. Knowles, and Christopher R. Dennison. A test bed to
examine helmet fit and retention and biomechanical measures of head and neck injury
in simulated impact. *Journal of Visualized Experiments*, 2017. (in-press at the time
of writing this thesis)

This publicaton focuses on development of an impact test bed, associated instru-
mentation, motion tracking system, and data analysis methods to quantify effects of
helmet fit on head and neck injury (nominally Chapters 2 - 4 in this thesis). The re-
maining chapters deal with the application of these methods in a study investigating
the effects of helmet fit on injury likelihood.

Chapter 2

Background

An overview of the fundamental topics in head and neck injury biomechanics are given in this chapter, as well as the current state of helmet protective assessment. A short summary of similar work investigating helmet fit on injury likelihood is also presented.

2.1 Head Injury

The portion of the human head that is protected by a helmet includes frontal, temporal, parietal and posterior aspects from the head vertex and then inferiorly to a horizontal plane passing through the auditory canals. Essentially, this comprises the upper head and its associated scalp (Figure 2.1). The scalp includes hair, skin, connective tissue, and muscle. Underneath the scalp is the skull, a structure of fused bones which serves to protect the brain. In between the skull and the brain there are several membranes and subarachnoid space. This subarachnoid space contains cerebrospinal fluid that surrounds and supports the brain. In head injuries, damage to the skull, brain, and other soft tissues are of concern.

Head injuries can be categorized as focal or diffuse injuries, but their occurence is not mutually exclusive. Brain injuries, which are associated with neurologic dysfunction, can occur with our without skull fracture. In fact, a skull fracture injury itself does not necessarily constitute neurological death or disability. Focal injuries
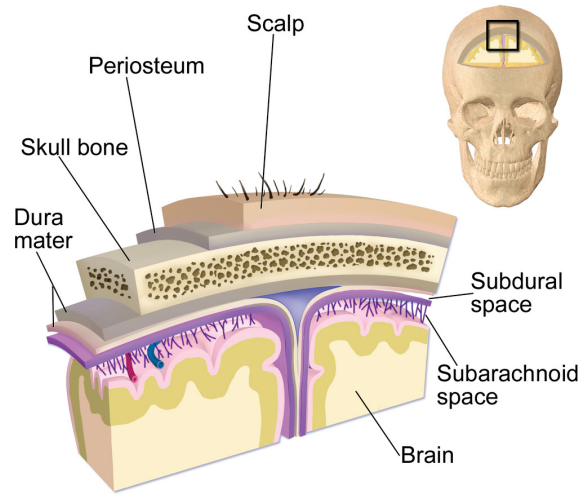
Figure 2.1: Layers Covering the Brain.

are usually associated with injuries in which the head is struck by an object and occur in a specific confined location with localized damage. Focal injuries include cortical contusion and hematoma, and account for two thirds of head injury deaths [14]. In contrast, diffuse injuries occur in a more widespread area, and are associated with acceleration or deceleration of the head. Physical contact with the head is not even necessary for diffuse injuries to occur. Diffuse injuries include mild TBI, such as concussions and although diffuse injuries account for only one quarter of head injury deaths, they are the most serious cause for neurologic disability [14]. The severity of injuries can also be classified with the use of the Abbreviated Injury Scale (AIS) [15]. Depending on the severity of an injury, a different AIS value can be assigned.

Whether an individual sustains a skull fracture, focal injury, or diffuse injury, is dependent on the biomechanical mechanism of injury [16]. In sports-related injury, this injury mechanism is commonly characterized as a rapidly applied mechanical impact to the head and can cause two types of phenomena. The first is a local deformation of the skull through to the brain causing focal injury. Severe focal injuries

tend to be associated with this linearly directed impact force, which can cause skull deformation, as well as contusion and bleeding in the underlying tissue. The severity of the impact is dependent on the magnitude, direction, area of impacting force, as well as the impact location. Accordingly, the most damage would result from a high magnitude force applied directly onto a thin section of skull over a small area and could cause skull fracture and cerebral contusion. Protective head gear aims to mitigate injury by reducing the loading magnitude and distributing load across the head. The second phenomena from an impact is caused by inertial effects of the head under acceleration or deceleration. This acceleration causes shear, tensile, and compressive strain within brain tissue to cause injury. Studies have shown that rotational loading, as opposed to translational loading, has a considerable role in these diffuse injuries [17, 18]. Diffuse injuries tend to be associated with this inertial loading and cause milder and diffuse brain injuries. These diffuse injuries, such as contusions and subdural hematoma, can be found outside the impact area [14]. Modern protective headgear (helmets) is sometime criticized in the lay-press and academic literature for not protecting the brain from diffuse injury [19, 20].

Much of biomechanical research for the head injury arises from automotive and sport research. Consequently, measures of impact severity were sought out in order to evalaute risk of injury. Important parameters for evaluating mechanical injury to the head include linear kinematics, angular kinematics, and localized pressure or force at the impact site [21].

One of the earliest and most common approaches in assessing head impact severity is measuring peak linear head acceleration, often represented in units of g (acceleration due to gravity, 1 g = 9.8 m/s^2). Consequently and intuitively, a head experiencing high linear accelerations would be expected to experience a more severe injury. In the 1960s, researchers from Wayne State University performed a series of animal and human cadaver experiments, investigating a human head's probability tolerance to

linear acceleration causing skull fracture [22]. Their results suggested a relationship between survivable injury with the linear acceleration experienced by the head and the time duration of acceleration experienced, shown in Figure 2.2. The line represents the demarcation between a fatal and survivable impact. Any combination of effective head acceleration and time duration of acceleration above the line would result in potentially fatal injury, and any combination below the line would result in a likely survivable impact. However, mild injuries would still be possible in the survivable range.
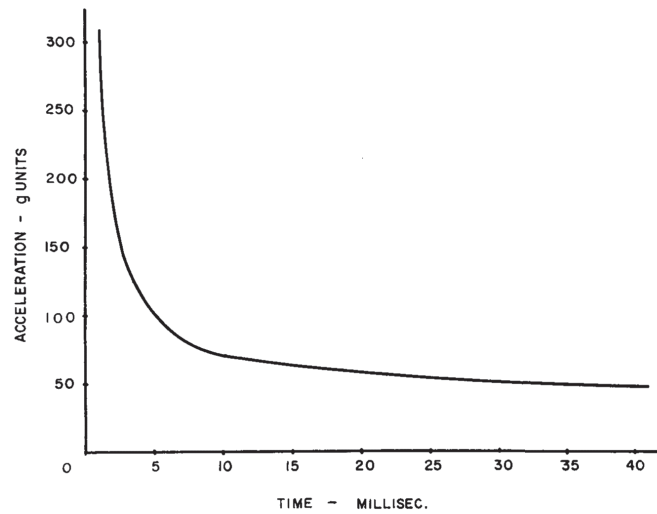
Figure 2.2: Wayne State Head Injury Tolerance Curve

Tolerance curve developed to assess head injury based on acceleration duration. Accelerations experienced above the line represent potentially fatal injuries while accelerations below the line represent likely survivable injuries [22]. Figure reproduced with permission from Gurdjian, Elisha S., V. L. Roberts, and L. Murray Thomas. "Tolerance curves of acceleration and intracranial pressure and protective index in experimental head injury." Journal of Trauma and Acute Care Surgery 6.5 (1966): 600-604.
(http://journals.lww.com/jtrauma/Citation/1966/09000/Tolerance_Curves_of_Acceleration_and_Intracranial.5.aspx)

Research proceeded to attempt to develop functions that describe the line shown in Figure 2.2. Several approximations to the line were proposed. Today, one of the most popular and widely referenced functions attempting to capture the tolerance presented by the Wayne State data is the head injury criterion (HIC). HIC (Equation 2.1) was proposed by the National Highway Trafic Safety Administration (NHTSA), and is commonly used in the automotive industry [23]. The function integrates acceleration

data in order to represent the duration that accelerations are experienced. The time window for calculating HIC is often chosen as 15 or 36 ms.

$$HIC = \left\{ \left[\frac{1}{t_2 - t_1} \int_{t_1}^{t_2} a(t)dt \right]^{2.5} (t_2 - t_1) \right\}_{maximum} \tag{2.1}$$

where

$$t_1 = \text{Arbitrary pulse start time [s]}$$
$$t_2 = \text{Arbitrary pulse end time [s]}$$
$$a(t) = \text{Acceleration over time [g]}$$

In helmeted impacts, the time duration is typically less than 15 ms [24]. Because the accelerations experienced by the head in most helmeted impacts are of similar duration, helmet certification simplifies a helmet assessment metric to ignore time duration and only measure peak linear acceleration, refered to as "peak g". In addition to HIC and linear acceleration, head injury assessment functions have continually been created and include factors such as angular acceleration, angular velocity, and even head mass. Some of these other functions include the Brain Rotational Injury Criterion (BRIC) [25], the Generalized Acceleration Model for Brain Injury Tolerance (GAMBIT) [26], and the Head Impact Power (HIP) [27].

Brain finite element models have also been developed to compute brain tissue strain in place of cadaver work. One brain model, known as the Simulated Injury Monitor (SIMon), can take kinematic inputs and find measures such as cumulative strain damage measure (CSDM) and maximum principal strain (MPS) [28]. These values in particular, were able to demonstrate the strong correlation between angular kinematics and brain tissue strains [29]. Because strain in brain tissue has been

correlated to anatomic injury and through these correlation efforts, severe brain injury in automotive impacts has been correlated to both CSDM and MPS. The connection between metrics like CSDM and MPS and brain injury has led these to be used in helmet assessment, as well.

Although there may be ongoing debate on the best head injury function, biomechanical research consistently suggests that both linear and angular kinematics play an important role. In order to best assess the likelihood of focal and diffuse injuries, both linear and angular kinematic measurements are necessary to fully portray the likelihood and type of head injury.

2.2   Neck Injury

The human neck is the most superior portion of the vertebral column, between the head and thorax. It serves to protect the spinal cord, and support the head and its movements. It is comprised of vertebral bones and soft tissue such as nerves, muscles, ligaments, and tendons. A column of 7 cervical vertebrae make up the neck (C1-C7), separated by intervertrebral disks, and houses the spinal cord. A complex network of joints, ligaments, and musculature grant flexibility and stability to the spine. Because of the complex structure of the neck, the underlying mechanisms of injury are not fully understood [16, 30, 31]. Neck injuries have a wide range of severity. Generally, injuries to the upper cervical spine are deemed more serious and are sometimes fatal. However, neck injuries include neck sprains, herniated disks, vertebral fractures, cervical dislocation, and spinal cord injuries.

Because the neck resembles a slender column, neck loading can be characterized with axial and bending loads. Injuries can often be categorized based on tension/compression and extension/flexion specifically. In impacts to the head, both compressive and bending loads may be present in the neck. The compressive load

is transmitted to vertebral bodies, pushing fragments of the vertebral body out and potentially causing spinal cord injury [32].
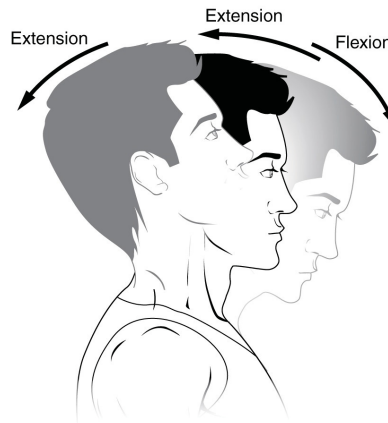
Figure 2.3: Neck Flexion and Extension

In understanding neck loading, neck bending in the form of neck flexion and extension is often considered alongside axial loading. This figure was modified under Creative Commons Attribution-Share Alike 3.0 Uported License. OpenStax College. Anatomy & Physiology, Connexions Web site. http://cnx.org/content/col11496/1.6/

Although neck forces and bending moments can be assessed individually, the combined loading and effects can also be assessed together. One such assessment method combining axial loading and bending effects is the Neck Injury Criterion (Nij) [33]. This criteria specifically examines the neck in tension or compression axial force combined with flexion or extension bending moment. By setting proposed critical limits for the neck, the normalized sum of forces and moments can be defined in Nij (Equation 2.2). These critical limits are based on volunteer, cadaver, and dummy tests [33] scaled for different neck sizes. Similiar to head injury metrics, Nij can also be associated with different AIS injury levels.

$$N_{ij} = \frac{F_z}{F_{int}} + \frac{M_y}{M_{int}} \qquad (2.2)$$

where

$$
\begin{aligned}
F_z &= \text{Axial Load [N]} \\
F_{int} &= \text{Critical Axial Load [N]} \\
M_y &= \text{Flexion/Extension Bending Moment [N.m]} \\
M_{int} &= \text{Critical Flexion/Extension Bending Moment [N.m]}
\end{aligned}
$$

These critical limits are different for different loading conditions. For axial loading, compression and tension have different limits and for bending, flexion and extension have different critical limits. Typically, Nij is determined using force and moment measurements from standardized anthropomorphic dummy models of the human. These models will be presented in a subsequent section (Section 2.4). In a Hybrid III, an upper neck load cell is often used for measurement of force and moment. The critical limts can be scaled for use with an anthropomorphic dummy such as 50th percentile male Hybrid III [23].

2.3   Methods in Helmet Assessment

Helmets are designed to protect against head injury by reducing the severity of an impact experienced by the head and with the increased use of helmets, fatal brain injuries have been dramatically reduced. However, the prevalence of mild traumatic brain injury (mTBI) still remains high [1]. In cycling, a helmet is usually comprised of three main components: an outer shell, an impact liner, and retention system (Figure 2.4). The outer shell serves to protect against penetration of sharp objects and distribute load across the impact liner. The impact liner serves to absorb as much of the impact energy as possible. Many helmets feature a crushable foam that

absorbs impact energy through deformation. By absorbing energy, the acceleration experienced by the head is effectively attenuated relative to an equivalent impact to a head that is not protected with a helmet. In cycling helmets, this deformation is plastic and renders the helmet effective for only a single impact. The retention system serves to retain the helmet on the head, to ensure protection throughout an impact. Ultimately, a helmet aims to limit impact force magnitude, and increase time-duration of impact, thereby resulting in lesser head acceleration than would be the case in a head impact to an unprotected head.
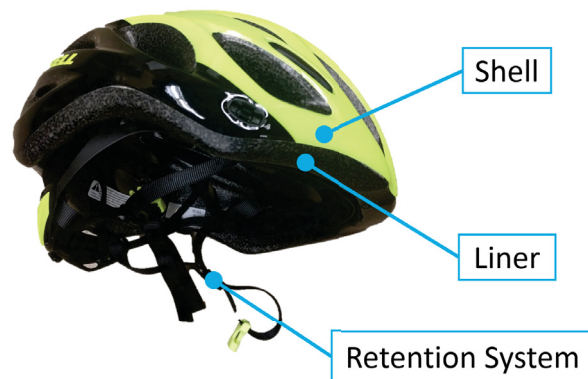
Figure 2.4: Cycling Helmet Components
The common components of a cycling helmet include a shell, liner, and retention system.

Certification of a helmet's protective ability is governed by various standards, such as ASTM (American Society for Testing and Materials), NOCSAE (National Operating Committee on Standards for Athletic Equipment), CPSC (Consumer Product Safety Commission), and CSA (Canadian Standards Association) [34, 11, 10, 35]. These standards specify the testing protocols for certifying a helmet and are based on peak linear acceleration measurement. As part of the specifying test protocols, details such as drop heights, impact velocities, anvil surfaces, and instrumentation requirements are specified. In each of these standards, a helmet is placed on a surrogate test headform which is then subject to free fall to impact an anvil. An accelerometer in the

headform measures the linear acceleration experienced by the headform during this impact (Figure 2.5). Depending on the standard, there exists different thresholds of allowable peak linear acceleration. For bicycle helmets, if the linear drop experiment results in head acceleration less than 300g, then the helmet protecting the surrogate head is considered to meet the minimum standard for impact attenuation (i.e. it passes the attenuation requirement) [10]. It should also be noted that none of these standards account for rotational acceleration.
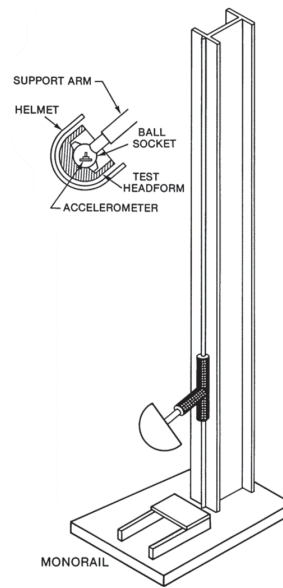
Figure 2.5: CSPC Helmet Drop Tower

In helmet assessment, an instrumented headform is accelerated in free fall into a hard anvil. A monorail design is depicted. Figure from CPSC Safety Standard for Bicycle Helmets. [10]

2.4   Methods in Injury Risk Assessment

Injury assessment in head injury often utilizes similar equipment to helmet assessment. Specifically, it is common to use a machine subjecting a headform free fall to impact an anvil while measuring acceleration. However, practices for injury assessment typically differ in the instrumentation and headform used. In addition to linear acceleration, angular acceleration can be measured through a gyroscope or calculated

from a linear accelerometer array. Head models that approximate the human head shape and mass distribution are also often used. These head models can also be coupled with neck models that attempt to recreate the motion that the human neck affords to the head. If angular acceleration is to be measured, it is important that a non-rigid neck be used. One such model used for head injury biomechanical research is the Hybrid III head and neck. In contrast to a magnesium headform that might be used in helmet assessment, a Hybrid III has features more similar to a human head. Specifically, a Hybrid III head has more realistic geometry, a vinyl skin, and non-rigid neck. This non-rigid neck allows angular kinematics to occur. Load cells can also be incorporated into the neck to measure neck kinetics at the OC/C1 or C7/T1 vertebrae. However, the Hybrid III is not without criticism. Compared to a human head, the Hybrid III still has geometric differences [36, 37]. The vinyl skin of the Hybrid III is also generally accepted to have a higher coefficient of friction compared to human skin, with some attempts at recreating an artificial human scalp [38]. The neck, although flexible, is still considerably stiffer than a human neck [39]. Despite these limitations, it is considered a repeatable and appropriate model to study effects on head mechanics of protective gear [40].
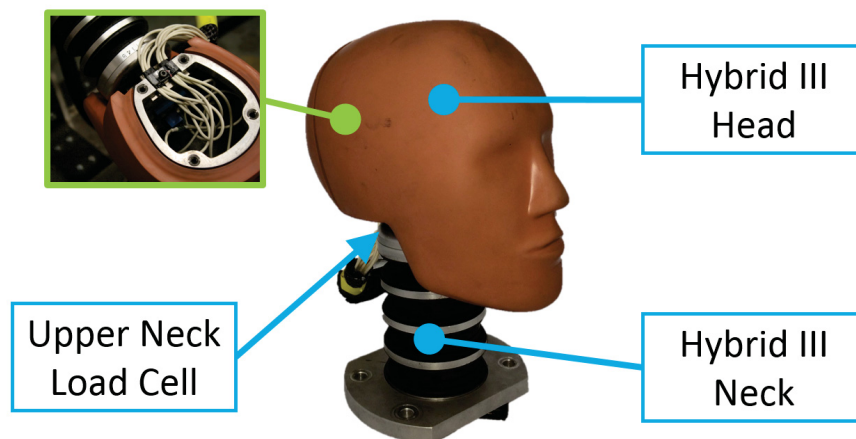
Figure 2.6: Hybrid III Headform and Neck

A Hybrid III Head and Neck can be equipped with a linear accelerometer array and upper neck load cell to determine head kinematics and neck kinetics.

Other headforms exist, such as the headform specified in the NOCSAE helmet standards. In contrast to the Hybrid III, the NOCSAE headform geometry is based on shape specifications based on cadaver heads. However, the Hybrid III head and neck are widely used in injury research, and although its limitations are well documented, there is a large body of research published using methods based on the Hybrid III. With the associated instrumentation, metrics used to assess focal/diffuse injuries can be determined to characterize injury severity and type.

2.5   Helmet Fit and Stability Evaluation

The protective efficacy of a helmet is dependent on helmet stability and retention. Helmet retention is important to adequately protect the head throughout the duration of an impact to ensure that the impact only contacts the helmet. Ideally, a helmet should protect the head for the initial impact and immediate subsequent impacts that may also occur in an accident. Helmet stability is often associated with helmet fit prior to impact. A well fit helmet should be appropriately positioned on the head and be resistant to movement. Assuming a helmet is adequately retained on the head, helmet fit could still have effects on helmet protective ability. Depending on the geometric interface between a head and helmet, the efficacy of a helmet liner in protecting a head could vary.

Standards also recognize the importance of helmet fit with a loose characterization of fit and stability tests [10]. Specifically, HPI (Helmet Positioning Index) and a stability test are often discussed. HPI is defined as the distance between the bottom brim of a helmet and the reference plane on a headform, and is generally established by the helmet manufacturer (Figure 2.7). However, this index serves more to indicate the proper wearing of the helmet, rather than quantifying fit. The stability test, sometimes called a roll off test, is a test procedure requirement for helmets to remain

on a head during impact. The protocol consists of applying a dynamic impact load on the edge of a helmet. If a helmet rotates excessively or comes off, the helmet fails the test (Figure 2.8). Whether or not this test is representative of a real impact is arguable. No other methods for quantifying helmet stability during impact exist in certification or research literature.
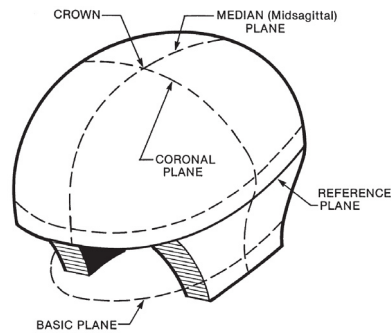
Figure 2.7: Test Headform for Helmet Certification

HPI is defined as the distance between the brow of a helmet and the basic plane on a headform. Figure from CPSC Safety Standard for Bicycle Helmets. [41]
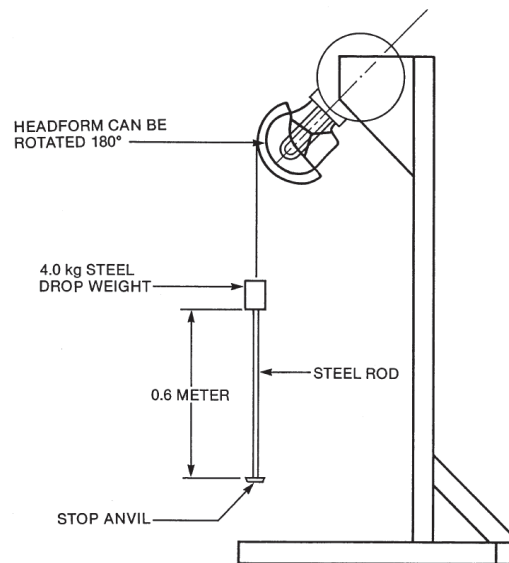
Figure 2.8: CPSC Stability Test

A test device for assessing helmet stability. A weight is dropped, acting as a dynamic load on the edge of a helmet. Excessive rotation results in the helmet failing the test. Figure from CPSC Safety Standard for Bicycle Helmets. [10]

2.6   Previous Research Examining Helmet Fit and Retention

Few studies have been performed in investigating the fitment of bicycle helmets in impacts. Helmet sizing has been investigated in a finite element analysis of motorcycle helmets [42], as well as simulated impacts for football helmets [12]. Both these studies suggest that appropriate helmet sizing has a role in injury risk. A slack or tight chin strap has also been investigated in simulated impacts with bicycle helmets [43, 44], with inconsistent conclusions on the importance of a tight retention strap. Finally, a backward fit case with a helmet improperly positioned on the head was simulated for bicycle helmets on preadolescents [44]. Interestingly, it was found that a poorly positioned helmet performed better in impacts to an angled surface.

These studies lack a full comprehension of the effect of bicycle helmet fit in regards to injury likelihood. Specifically, only studies concerning helmet retention systems and helmet positioning in one impact condition have been performed with the focus of bicycle helmets. Studies do not exist in studying helmet fit while considering helmet sizing and helmet positioning in a variety of impact scenarios. Further study investigating the effect of helmet fit on injury likelihood would be able to expand and validate existing studies. In this thesis, both helmet sizing and helmet position will be considered in different impact scenarios. Existing methods for determining biomechanical measures of injury risk will be carried out, while implementing new methods in quantifying fit and tracking dynamic helmet movement.

Chapter 3

Fit Force Transducer for Objective Fit Measurement

A new method of quantifying helmet fit based on optical sensors is discussed in this chapter. A brief overview of in-Fibre Bragg Grating (FBG) theory and the design of a transducer to measure helmet fit forces are presented. The application and evaluation of this fit measurement method are also presented.

3.1 Helmet Fit Assessment

Although, poor helmet fit is often associated with increased risks of injury in crash [5, 6, 7], a good fit is often subjective and inconsistently defined. Hypothetically, a good helmet fit would translate into good helmet stability and retention during impact. However, measures of objectively quantifying helmet fit are limited. In academia, some methods exist to characterize helmet fit and consider parameters such as geometry or force to characterize helmet fit [12, 13]. Ellena et al proposes the Helmet Fit Index (HFI) that quantifies the similarity in geometry between head shapes and helmet liners, defining similarity in geometry as a good fit [13]. With 3D scanning, the gap between a head and inside of a helmet was analyzed and a HFI was computed. Similarly a local HFI was also computed at the front, top, right, left,

and back areas of the head. Establishing similarity of geometry between head and helmet infers that the helmet is fit well. In Jadischke's work, a "fit cap" was created with an array of Tekscan pressure indicating film sensors [12]. By placing this fit cap between a head and football helmet, the pressure distribution of the fit could be examined. The helmet fit force sensors in this thesis were made with a similar goal as Jadishke's work, in quantifying helmet tightness in the form of fit forces. Presumably, a relationship exists between tightness and helmet retention and head protection.

3.2   Fit Force Sensor Design

In order to quantify helmet fit, fit force sensors were designed to characterize the tightness of a helmet. The rationale behind measuring force is that a relationship exists between helmet tightness and helmet retention. By quantifying the tightness as a force, a representation of helmet retention and head protection may be determined. This insight would allow helmet retention ability to be estimated, as well as quantitatively comparing different fit scenarios. The sensors were designed to be unobtrusive, repeatable, and sensitive to static forces in the range of 0 - 50 N. Designing an obtrusive sensor was important so that the contact between the head and helmet characterizing fit would be unaffected by the presence of fit sensors. The concept of these sensors is similar to Jadischke's sensors [12], in that force is measured at different points on the head. The design of the sensor for fit force measurement is based on a sensor used to study impact force in head impacts by Butz et al [45, 46, 47], due to their good response, repeatability, and unobtrusiveness. Modifications to the original design were made in order for the sensor to better suit fit force measurement. Specifically, the sensitivity was increased for lower forces and thickness was decreased to further minimize interference with fit.

21

3.2.1 In-Fibre Bragg Grating Theory

Optical fibers are thin flexible fibers, made from glass or plastic, used to transmit light between two fiber ends. FBGs are structures that can be produced in an optical fiber, consisting of periodic variations of refractive index within the core of the fiber. These gratings act like a series of partially reflective mirrors that reflect only a selective wavelength of light. The specific wavelength of light reflected back up the fiber is dependent on the periodic spacing of gratings. This reflected wavelength is called the Bragg wavelength, λ_B. The remaining light propagated down the optical fiber continues through the FBG (Figure 3.1).
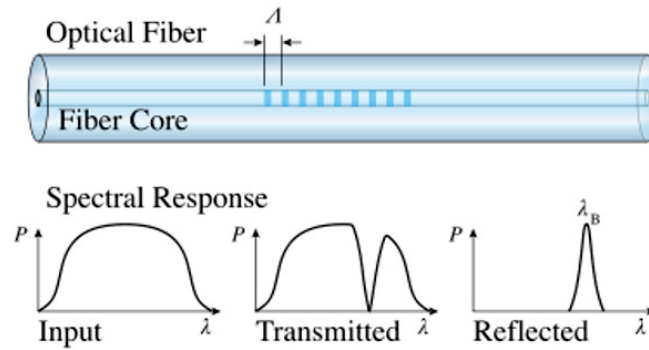
Figure 3.1: in-Fibre Bragg Grating Schematic

Modified from Wikipedia.org under GFDL License

The Bragg wavelength is dependent on the grating period and grating index of refraction (Equation 3.1). Different indices of refraction in the fiber are denoted by n_0, n_1, ... n_3.

$$\lambda_B = 2\Lambda n_0 \tag{3.1}$$

where

$$\Lambda \quad = \quad \text{Grating Period [nm]}$$

$$n_0 \quad = \quad \text{Grating Index of Refraction}[--]$$

In communications, this transmission of light can be used to send data encoded into the propagated light. FBG structures can then be used to extract certain wavelengths of light. However, FBGs can also be used as a sensing device for strain and temperature measurement capabilities. They have been becoming more popular in biomechanical research, due to their size, biocompatability, chemical inertness, invulnerability to electrical interference, and multiplexing ability [46, 48].

When the fiber is subject to a strain, the grating period and refractive index are varied, resulting in a change in Bragg wavelength. The change in wavelength can then be used to predict change in axial strains (Equation 3.2), with a strain sensitivity coefficient, S_ε.

$$\Delta\lambda_B = S_\varepsilon\varepsilon \tag{3.2}$$

where

$$\Delta\lambda_B \quad = \quad \text{Bragg wavelength shift [nm]}$$

$$S_\varepsilon \quad = \quad \text{strain sensitivity [nm/microstrain]}$$

$$\varepsilon \quad = \quad \text{axial strain [mm/mm]}$$

Ultimately, a FBG can be used as a strain sensor. By employing a transducer,

a force can then be related to the strain or wavelength shift. Several characteristics make FBGs suitable for this application, including their small size and multiplexing capability. In the context of helmet fit, their small size allows for easy integration into materials with minimal interference on helmet fit. The multiplexing ability comes from the ability to write FBGs with different grating periods along the same optical waveguide. The different FBGs will then selectively reflect a different wavelength of light corresponding to the number of different grating periods. This multiplexing ability is beneficial because it allows for more sensors to be included within a small space. Multiple FBGs can be written on one optical fibre, allowing a single fibre to both supply light and sense strain. In contrast, electrical strain gauges require 4 wires per gauge. This multiplexing allows a simpler design, as well as less clutter to further minimize interference on helmet fit.

3.2.2   Transducer Design

The transducer of the final design is comprised of 3D printed and aluminum parts with an FBG sensor (Figure 3.2).
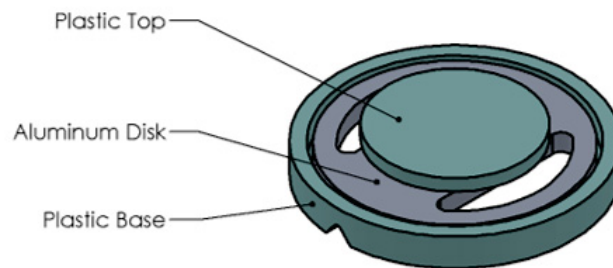
Figure 3.2: Fit Force Transducer

(The fit force transducer consists of two 3D printed plastic components, and one aluminum component. Strain on the aluminum component is measured with a FBG. The plastic filament used is a blend of PLA (polylactic acid) and PHA (polyhydroxylalkanoate).

This transducer functions on the principles of a simple beam with supported ends. By applying a load on the top surface of the transducer (Figure 3.3a), a force on the

aluminum beam causes a strain on the underside of the beam (Figure 3.3b). This strain is then measured by an FBG fixed to the bottom of the beam (Figure 3.3c). Depending on the geometry and material properties of the beam, the same force can create different amounts of strain. Effectively, the sensitivity of force measurement can be tuned by changing the geometry of the transducer. An in-depth study of the sensor design analysis, including a linearity and frequency analysis is performed in Butz's thesis [47].
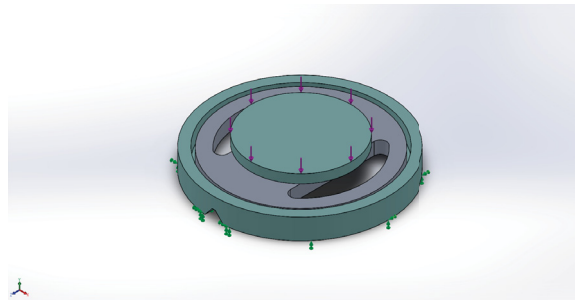
(a) Transducer Loading
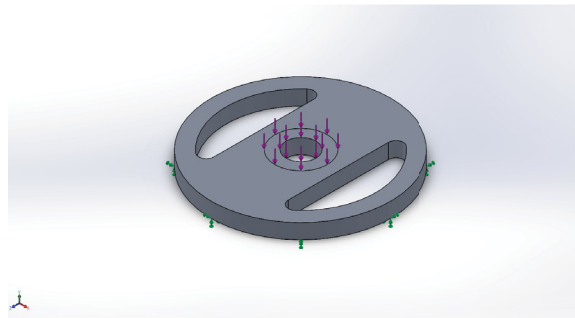
(b) Aluminum Disk Loading

(c) Beam Loading Simplification

Figure 3.3: Transducer Loading Conditions

With a transducer applying strain on an FBG, a force can then be correlated from Bragg wavelength shifts (Equation 3.3) with a transducer sensitivity, K. The

transducer sensitivity can be adapted to function at different force ranges for different applications by changing the aluminum beam geometry.

$$F = K\Delta\lambda_B \tag{3.3}$$

where

$$
\begin{aligned}
F &= \text{Applied Force [N]} \\
K &= \text{Transducer Sensitivity [N/nm]}
\end{aligned}
$$

In order to produce a suitable sensor, transducer designs were iterated and evaluated. With 3D printed plastic and waterjet-cut aluminum parts, the transducer could be rapidly prototyped. The assessment of the sensor was performed with calibration.

3.2.3 Sensor Fabrication

The sensors were designed with ease of fabrication in mind. The sensing component consists of two plastic components, one aluminum disk, and a FBG. The main transducer component was an aluminum disk, waterjet-cut out of 6061 sheet stock. This allowed satisfactory dimensional tolerancing and material consistency. The plastic components were rapid prototyped with a 3D printer using a filament blend of PLA (polylactic acid) and PHA (polyhydroxylalkanoate). These plastic components served to direct load to the center of the aluminum disk and provide support. Because the material properties of these components were not critical, problems with anisotropy of the 3D printed part were avoided. All parts were adhered with cyanoacryalte. An FBG was then fixed to the bottom of the aluminum disk, with the grating centered at the center of the aluminum disk. The final sensor design has a thickness and diameter

of 2.6 mm and 14 mm respectively.
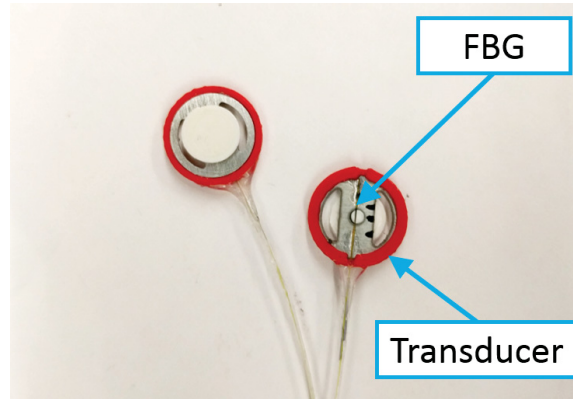
Figure 3.4: Fit Force Transducer

The top (left) and bottom (right) of a fit sensor are shown. A FBG is also shown fixed to the bottom of the transducer. Each sensor has a thickness and diameter of 2.6 mm and 14 mm respectively.

Five sensors were then multiplexed with optical couplers to combine multiple sensors on the same channel. This allowed sensing at 5 locations on the head.

3.2.4 Transducer Static Calibration

To calibrate a sensor, known masses were loaded onto the sensor and the Bragg wavelengths were measured. A SmartSoft interrogator (Smart Fibres Ltd, United Kingdom), sampling at 2.5 kHz was used for data acquisition of Bragg wavelength. The average wavelength over 3 seconds was recorded. A relationship between mass and wavelength shift could then be determined. Equivalently, the relationship between force and wavelength shift could be calculated (Figure 3.5). To calibrate each sensor, calibration masses were incrementally added on the sensor with the Bragg wavelength recorded, and then similarly removed. This procedure was repeated three times for each sensor. A linear regression analysis was then performed to determine the sensitivity and consistency of each sensor. In total, 5 sensors were fabricated and calibrated (Table 3.1).

27
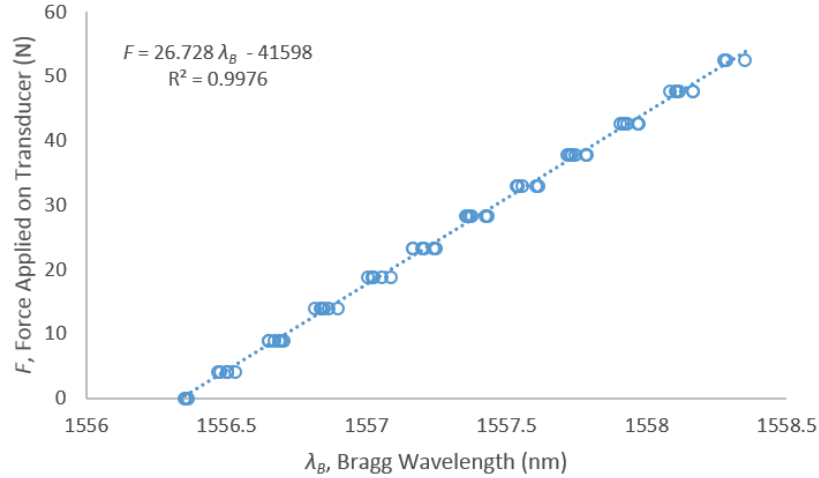
Figure 3.5: Fit Force Calibration

Each sensor was calibrated by incrementally increasing calibration masses placed on the sensor then decreasing the calibration masses. This procedure was repeated three times, then regression was used to determine the corresponding slope. The calibration of Sensor 1 is shown.

Table 3.1: Fit Force Sensor Calibration

Sensor	Sensitivity (N/nm)	R^2
1	26.73	1.00
2	20.39	0.99
3	15.05	1.00
4	17.03	1.00
5	19.02	0.99

3.3 Fit Forces Between Different Fit Scenarios

These fit sensors were then used in evaluating the different fit forces in 4 fit scenarios (Table 3.2) on a Hybrid III 50th percentile male headform with a head circumference of 575 mm. These fit scenarios were based on definitions of correct helmet use from epidemiological studies [7], which commonly included helmet size and position as parameters for good fit. Specifically, correct helmet positioning was defined as not covering the eyebrows or exposing the forehead. A *Normal* fit uses a correctly sized helmet and the helmet positioned with approximately two finger widths of space be-

tween the helmet brim and headform forehead. An *Oversized* fit uses an Extra Large helmet to represent the variation in helmet sizing. The *Forward* fit uses a correctly sized helmet, but positioned forward with the helmet brim just above the eyes. The *Backward* fit also uses a correctly sized helmet, but positioned backward to expose the forehead. The forward and backward fit scenarios were chosen as the maximum variations in helmet positioning that were still felt to represent plausible use with regular individuals. For instance, it was deemed unlikely that an individual would position a helmet to cover his/her eyes. A CPSC certified helmet (Bell Traverse), available in two sizes, was used for all fit scenarios. According to the helmet manufacturer's provided fit guide, the head circumference of a Hybrid III 50th percentile headform would most appropriately fit a Universal helmet. However, the circumference range of a Hybrid III also fell within the appropriate range for an Extra Large helmet. Other fit parameters were kept consistent: the chinstrap was tightened to leave approximately one finger width of space under the chin, and the adjustable retention strap was hand tightened to keep a secure fit.

Table 3.2: Helmet Fit Force in Different Fit Scenarios

Fit Scenario	Helmet Size	Helmet Angle
Normal	Universal	Normal
Oversized	Extra Large	Universal
Forward	Universal	Forward
Backward	Universal	Backward

3.3.1 Fit Force Measurement Experimental Protocol

The same optical interrogator previously used in calibration was used for fit force evaluation. Five fit sensors were arranged on the Hybrid III Head, on the front, back, left, right and top (Figure 3.6). These sensors remained in the same location for all fit scenarios. Because the wavelength shift was being measured, a reference measurement with the transducers on the un-helmeted headform was taken. This was performed

prior to every measurement. The helmet fit scenario was then arranged on the head-form and the measurement was taken. For all Bragg wavelength measurements, the interrogator was set to a sample rate of 2.5 kHz. The average Bragg wavelength over 3 s was then taken. For each helmet fit scenario, the same measurement procedure was repeated 6 times by removing and replacing the helmet. The fit sensors were not removed. With previous calibration data, the fit force could then be determined from wavelength shift.

Fit forces were measured on an inverted Hybrid III headform. Measurements could also have been performed with the headform upright, which could result in higher measured forces at the head vertex. However, the quantification of change in forces between fit scenarios was the focus. Whether the head is upright or inverted would have no difference on relative change in fit force.
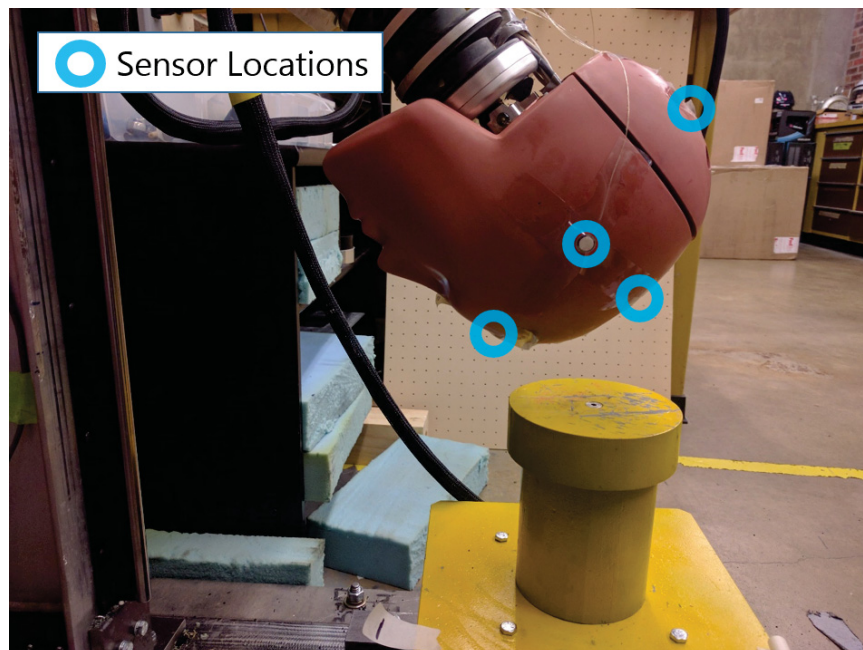
Figure 3.6: Sensor Locations

Fit sensors were placed on the Hybrid III head top, left, right, front, and back sides. Copyright Journal of Visualized Experiments. Yu, H., Knowles, B., and Dennison, C.. A test bed to examine helmet fit and retention and biomechanical measures of head and neck injury in simulated impact.

3.3.2   Results

The helmet fit forces were determined for each fit scenario at each individual location (Figure 3.7). A t-test, assuming unequal variances, was also performed to determine significant differences in measured force (p $<$0.05). Higher force measurements imply a tighter fitting helmet. An oversized helmet was shown to only have significantly lower fit forces on the top of the head. The forward fit helmet was shown to exhibit significantly higher fit forces on the front of the head. On the left and right sides of the head, statistically significant differences were observed for the forward and backward fit scenarios. For all scenarios, the sensor on the back of the head did not experience significantly different fit forces.
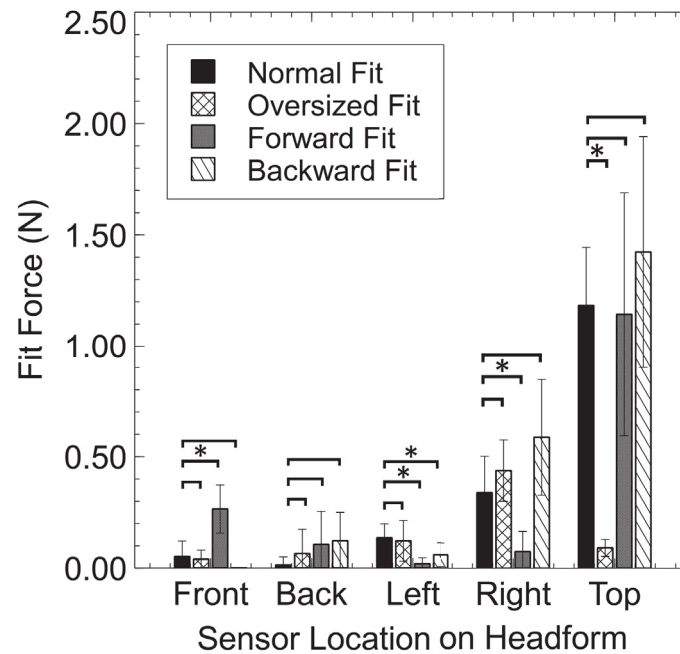
Figure 3.7: Fit Forces Between Different Fit Scenarios

Standard deviations of measurements are represented with error bars. Significance is also shown for p $<$0.05 (*).
Copyright Journal of Visualized Experiments. Yu, H., Knowles, B., and Dennison, C.. A test bed to examine helmet fit and retention and biomechanical measures of head and neck injury in simulated impact.

The fit forces between the different scenarios could also be expressed as a global fit force and global fit force deviation to characterize the overall tightness of a helmet

(Table 3.3). Calculation of these metrics is outlined in Appendix A. The global fit force represents the average force exerted on the head while the global fit force deviation represents the variation of this force across different sensor locations. A tighter helmet would be represented by a higher global fit force. A helmet exerting consistent fit force across the head would then exhibit a very low deviation. A t-test was also performed to show only an oversized helmet exhibited significantly smaller global fit forces.

Table 3.3: Helmet Fit Force in Different Fit Scenarios.

Fit Scenario	Global Fit Force (N)	Global Fit Force Variation (N)
Normal Fit	0.35 ± 0.09	0.49 ± 0.10
Oversized Fit	$0.15^* \pm 0.05$	$0.18^* \pm 0.06$
Forward Fit	0.32 ± 0.21	0.49 ± 0.21
Backward Fit	0.44 ± 0.23	0.61 ± 0.23

The global fit force can be represented as an average of fit forces across all sensors, with the global fit force variation representing the variation in fit force. A t-test was also performed to determine scenarios with a significantly different global fit force, $p < 0.05$ (*).

The helmet fit sensors were capable of distinguishing significantly different fit forces between different helmet fit scenarios, with forces on the range of 0 - 2 N. Occasionally, force measurements of zero were recorded due to no contact between the sensor and the helmet. This was caused by either a gap of separation between the head and helmet due to dissimilar geometry or the sensor being positioned underneath a helmet vent.

3.3.3 Discussion

Using global fit force to describe the overall tightness shows that only an oversized helmet exhibited lower tightness, as expected. However, these difference in tightness were primarily due to the small fit force recorded on the top of the head. The retention system was able to produce similar fit forces as the other fit scenarios at the other locations on the head. The lower overall tightness may suggest poor helmet

retention for the oversized helmet, but because the lower global fit force is primarily due to the force measurement at a single location, retention may not be significantly affected. Compared to a normal fit, both the forward and backward fit showed similar tightness. Because the helmet is the same size for these scenarios, this is anticipated. With similar tightness, both the forward and backward fit scenarios may be expected to show similar levels of helmet retention.

The fit force sensors were capable of distinguishing significantly different fit forces between different fit scenarios at different locations. However, using different locations to analyze fit forces may require precise attention to sensor locations. As expected, a forward fit exhibited more force to the front of the head relative to a normal fit scenario. In contrast, the fit force at the back did not show significant changes between any fit scenarios. This suggests that different locations on the head may have different sensitivities to fit scenario. The results for this particular helmet suggests that front of the head may experience significantly different fit forces while the back may not. These differences are likely due to the geometry of the head and helmet. However, the difference in sensitivities would show that a single sensor is insufficient in determining trends in tightness between different fit scenarios. Between different headforms and helmets, these results would likely differ. Significant differences in fit force were also noted in the left and right sensors for the forward and backward fit scenarios. It would be expected that the left and right sensor exhibit the same results due to symmetry. However, the left and right sensors were positioned visually, so their exact positions may not have been perfectly symmetric. As a result, the different locations of the sensors could cause different interference between the head and helmet. The differences between the left and right sensor show that visual alignment of sensors may be insufficient and cause variations in fit force measurements. Despite appearing symmetric, the small differences in position were capable of producing different results.

The limited spatial resolution of the fit force sensor array may be a limitation. A 5-sensor array may not fully represent the distribution of force across the head. Because the design of bicycle helmets often includes open vents, a sensor may be placed underneath a vent and not make contact with the helmet. As such, the sensor measures zero force and potentially further misrepresent helmet tightness. In order to mitigate the event of a zero force reading, the sensors could have been placed on the helmet instead of the head. However, the sensors were placed on the head to maintain consistency and repeatability of the experiment. Placing sensors on the helmet would require a new protocol for different helmets. Another potential solution to better represent the distribution of force across the head is to expand the number of sensors. With the small size of the sensors and multiplexing ability of FBG sensors, a greater number of sensors could be feasibly distributed around the head. Increasing the number could give a better representation of average tightness, as well as discern locations of high and low fit force fluctuations to provide further insight on helmet stability. With the ability to detect regions of contact between the head and helmet, increasing spatial resolution also allows the contact area between the helmet and head to be considered. In addition to the magnitude of force exhibited on the head by a helmet, the amount of contact area may also be valuable in characterizing fit.

The fit sensors in this study were capable of determining differences in fit forces between different fit scenarios, which could also be communicated as the tightness of a helmet. However, the measured fit forces were relatively low, on the scale of several newtons, which suggests the tightness between the head and helmet liner may not be the most valuable measure for quantifying helmet fit in bicycle helmets. Other factors may play a more important role in quantifying helmet fit, such as the amount of contact area between the head and helmet, the tightness of the retention strap only, or the similarity in geometry between the head and helmet.

CHAPTER 4

TRACKING HEAD-HELMET DISPLACEMENT

A new method of quantifying helmet stability is discussed in this chapter. The application and capabilities of the method are investigated. In Chapter 5, Head-helmet displacements in simulated impact will be presented and discussed.

4.1 Cinematography in Biomechanics

Using cinematographic equipment to analyze kinematic parameters of a body is a common tool in biomechanics laboratories. From each still frame of a video, a 2-dimensional pixel coordinate system can be used to describe the position of a point. With calibration and a scaling factor, the coordinates of this point can then be converted into physical dimensions. In combination with camera frame rate, kinematics like velocity and acceleration may be determined. With multiple cameras, the kinematic analysis can be expanded from planar to spatial motion. High speed cameras in particular can also be incorporated to capture events occurring at high speeds. Cameras can even be synchronized with other equipment, such as load cells, to more fully understand the dynamics of an event. For studying head injury and impact, the use of multiple high speed cameras can be quite valuable. Moreover, the capabilities of multiple high speed cameras in studying head impacts has been previously proven [31].

4.2   Head-Helmet Displacement

The ability to track helmet movement could prove to be a valuable tool in evaluating the retention ability of a helmet. A helmet that covers and protects the head throughout an impact can be deemed more effective than one that does not, and can be revealed by analyzing a helmet's relative motion. One potential method of quantifying helmet position is taking the distance between the helmet brim and forehead, similar to HPI (Figure 4.1). In order to track head-helmet displacement, a new method utilizing high speed cinematography was developed to track this distance. This method uses two high speed cameras to track points on a head and helmet. The conversion of these points into 3D space is achieved with the Direct Linear Transform (DLT) method [49]. Because the points on the helmet brim and forehead are not easily visible throughout an impact, these points are determined indirectly. The calculations performed to determine these points utilize a Singular Value Decomposition (SVD) method [50].

Figure 4.1: Head Helmet Displacement Vector

The vector used to describe head helmet displacement is the line between a point on the helmet brim and head forehead, similar to HPI. The absolute value of this distance is head-helmet displacement.

4.3 Determining Point Locations in 3D Space

By performing motion tracking on video footage, the 2-dimensional pixel coordinates of a point may be determined. With a scaling factor, these coordinates can be transformed from pixel co-ordinates to phyysical co-ordinates in a cartesian reference frame. However, this scaling only works when motion occurs in a plane parallel with the camera sensor. In order to determine 3-dimensional coordinates of spatial movement with depth, another view of the object must be achieved. Prisms and mirrors can be used to obtain a second view, but the simplest setup adds a second camera. The use of a second camera is presented. One method of determining the 3-dimensional coordinates of a point from two 2-dimensional sets of data is called the DLT method [49].

4.3.1 Direct Linear Transform Method

The DLT method requires two steps.

1. Calibrating the space to find a transformation matrix for each camera

2. Applying the transformation matrices to 2-D pixel coordinates (u, v), in order to find 3-D spatial coordinates (x, y, z)

Two coordinate systems must be defined for this method: a 2-dimensional image plane coordinate system and a 3-dimensional spatial coordinate system. The 2-dimensional coordinate system refers to the coordinates from an image captured by a camera. The vertical and horizontal component of this coordinate system is often denoted as u and v respectively, often measured in pixels. The 3-dimensional system refers to the real 3-dimensional space and is denoted as x, y, and z. These spatial coordinates are measured in units of real lengths, such as meters. The DLT method ultimately converts between the two coordinate systems, $[u, v]$ from each camera and

$[x, y, z]$ in real space.

With the DLT method, the projection of points in 3-D spatial space onto a 2-D image plane can be expressed in Equations 4.1 and 4.2.

$$u = \frac{L_1 x + L_2 y + L_3 z + L_4}{L_9 x + L_{10} y + L_{11} z + 1} \tag{4.1}$$

$$v = \frac{L_5 x + L_6 y + L_7 z + L_8}{L_9 x + L_{10} y + L_{11} z + 1} \tag{4.2}$$

where

$$
\begin{aligned}
u, v &= \text{Horizontal and vertical coordinates in image plane (px)} \\
x, y, z &= \text{3-D coordinates in real space (m)} \\
L_1, L_2, ..., L_{11} &= \text{Transformation coefficients, determined through calibration}
\end{aligned}
$$

Equations 4.1 and 4.2 represent the relationship between coordinate systems for an individual view or camera. As such, 2-D coordinates for a two camera setup can be further specified as u_L and u_R to reference a camera on the left and right. In addition, each camera also has a unique set of transformation variables. For a two camera setup, the same variables, L, could be used to denote the transformation $(L_1, L_2, ..., L_{11})$ for one camera and R can be used to denote the transformation variables for another camera $(R_1, R_2, ..., R_{11})$. In order to find these transformation coefficients, L and R, calibration must be performed. The calibration process requires that for a set of points, the 3-D spatial coordinates must already be known. Taking the 2-D pixel coordinates of these points recorded by each camera and the known 3-D coordinates, the transformation matrices for a camera can be determined (Equation 4.3). Since each point generations 2 equations, at least 6 calibration points must be defined to

determine the 11 unknown coefficients.

$$
\begin{bmatrix}
x_1 & y_1 & z_1 & 1 & 0 & 0 & 0 & 0 & -u_{L1}x_1 & -u_{L1}y_1 & -u_{L1}z_1 \\
0 & 0 & 0 & 0 & x_1 & y_1 & z_1 & 1 & -v_{L1}x_1 & -v_{L1}y_1 & -v_{L1}z_2 \\
x_2 & y_2 & z_2 & 1 & 0 & 0 & 0 & 0 & -u_{L2}x_2 & -u_{L2}y_2 & -u_{L2}z_2 \\
0 & 0 & 0 & 0 & x_2 & y_2 & z_2 & 1 & -v_{L2}x_2 & -v_{L2}y_2 & -v_{L2}z_2 \\
\vdots & \vdots & \vdots & \vdots & \vdots & \vdots & \vdots & \vdots & \vdots & \vdots & \vdots \\
x_N & y_N & z_N & 1 & 0 & 0 & 0 & 0 & -u_{LN}x_N & -u_{LN}y_N & -u_{LN}z_N \\
0 & 0 & 0 & 0 & x_N & y_N & z_N & 1 & -v_{LN}x_N & -v_{LN}y_N & -v_{LN}z_N
\end{bmatrix}
\begin{bmatrix} L_1 \\ L_2 \\ \vdots \\ L_{11} \end{bmatrix}
=
\begin{bmatrix} u_{L1} \\ v_{L1} \\ u_{L2} \\ v_{L2} \\ \vdots \\ u_{LN} \\ v_{LN} \end{bmatrix}
\tag{4.3}
$$

or

$$[M][L] = [U] \tag{4.4}$$

where

$$N \quad = \quad \text{Number of Points used for Calibration}$$

Equation 4.3 can also be represented in matrix form (Equation 4.4). $[L]$, the calibration coefficients, may then be solved with the method of least squares. Although a minimum of 6 points are required, more may be included to increase redundancy and improve accuracy. These points should be spread throughout the control volume of interest.

From the calibration procedure, the transformation matrices for each view, $[L]$ and $[R]$, may be determined. In combination with new 2-D coordinates, these transformation matrices can be applied to find the corresponding 3-D spatial coordinates (Equation 4.5).

$$\begin{bmatrix} L_1 - L_9 u_L & L_2 - L_{10} u_L & L_3 - L_{11} u_L \\ L_5 - L_9 v_L & L_6 - L_{10} v_L & L_7 - L_{11} v_L \\ R_1 - R_9 u_R & R_2 - R_{10} u_R & R_3 - R_{11} u_R \\ R_5 - R_9 v_R & R_6 - R_{10} v_R & R_7 - R_{11} v_R \end{bmatrix} \begin{bmatrix} x \\ y \\ z \end{bmatrix} = \begin{bmatrix} u_L - L_4 \\ v_L - L_8 \\ u_R - R_4 \\ v_R - R_8 \end{bmatrix} \quad (4.5)$$

or

$$[P][g] = [Q] \quad (4.6)$$

Again, Equation 4.5 can also be represented in matrix form (Equation 4.6). With the least squares method, $[g]$ may then be solved to determine spatial coordinates, $[x, y, z]$.

By maintaining the same camera setup, the DLT method can then be applied to each frame of a video by utilizing the same transformation matrix to find spatial coordinates. After using DLT to find the spatial coordinaets, the known change in time between consecutive images can be used to estimate other kinematics such as velocity and acceleration. In the DLT method discussed, 11 transformation coefficients are determined. In order to account for optical distortions, additional parameters could also be included in the transformation matrix $[L]$. However, more calibration points would be required.

4.3.2 Accuracy of Direct Linear Transform Method

In order to evaluate the accuracy of motion tracking and the DLT method in tracking helmet movement, a simple accuracy analysis is performed with a headform impact. The DLT method is used to track two points on the headform, separated by a known distance of 15 mm. The deviation from this distance is measured. Two Phantom v611 cameras (Vision Research, NJ) are arranged around a custom built helmet impacting tower (Figure 4.2). Each camera is equipped with a 50 mm f/1.4 lens (Carl Zeiss, Germany), with the aperture set at f/1.4. The cameras are also synchronized with

the frame rates set to 1000 fps.
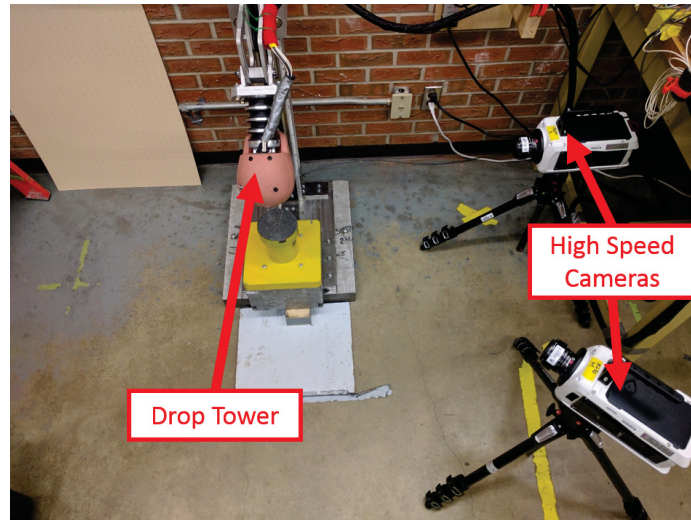
Figure 4.2: High Speed Camera Configuration

Two high speed cameras were configured around the drop tower. One was placed to the side and the other was placed approximately 45°. Copyright Journal of Visualized Experiments. Yu, H., Knowles, B., and Dennison, C.. A test bed to examine helmet fit and retention and biomechanical measures of head and neck injury in simulated impact.

A calibration cage with 18 calibration markers was previously designed (Figure 4.3). The geometry of the calibration fixture was designed to reasonably fill the control volume being recorded, with the calibration markers spread uniformly throughout. Using a Coordinate Measuring Machine (Mitutoyo, Japan), the spatial coordinates of these markers were determined. The locations of each point were determined with an average variance of 0.099 mm. Prior to the experimental impacts, the space is calibrated with this calibration fixture. Phantom Camera Control (PCC) Software is used to obtain 2-D image space coordinates of these calibration points from each camera. The DLT method can then be used to find transformation coefficients.

After the space is calibrated, two markers are placed on the head with known separation distance of 15 mm. A drop can then be performed. Using PCC software, the 2-D pixel coordinates of these markers throughout impact are obtained. The difference between the known distance and calculated distance between these two points is interpreted as a representation of the error. A drop was repeated 10 times
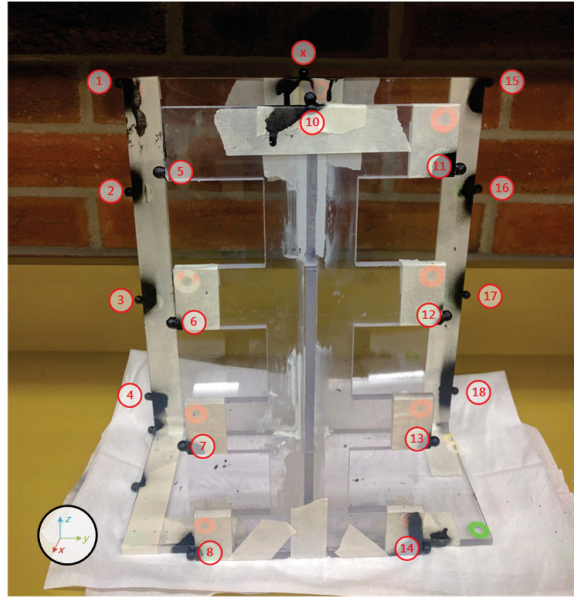
Figure 4.3: Calibration Cage

A calibration cage with known point locations was used to calibrate the space for the DLT method. The calibration frame fills a control volume measuring 12.0 x 10.0 x 5.0 ".

(Figure 4.4) to show variability. Error was tracked for 250 msec, which is much longer than the duration of an impact.
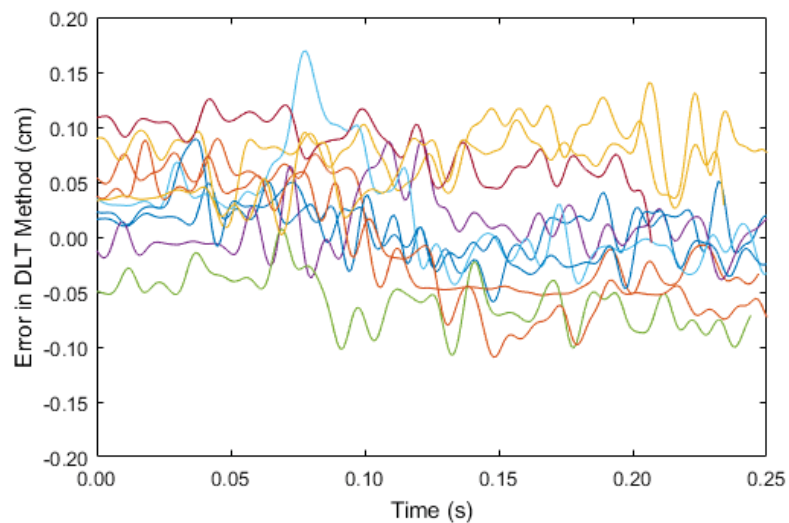
Figure 4.4: DLT Error

The error in the DLT method was determined for 10 helmeted drops. This error is defined as the difference between the known distance between two points and the calculated. Each line represents the error for a single drop.

Throughout all the drops, the error consistently ranges from approximately -0.10

cm to +0.15 cm. Because helmet movement in the millimeter magnitude are negligible in assessing helmet stability, these errors are deemed reasonable.

4.4 Indirect Point Tracking

To quantify relative movement between the head and helmet, we define a vector. The vector of interest measures the distance between the helmet brim and forehead. However, these two points are not consistently visible during an impact and cannot be directly tracked. For this reason, the head and helmet are tracked as bodies instead and the position of each the forehead and helmet brim are calculated. In other words, the forehead location and helmet brim locations are tracked indirectly. In order to track either the forehead or helmet brim, the same method is performed. For the helmet, 3 points are tracked during impact. By taking a reference frame prior to impact, the location of the helmet brim relative to the tracked markers can be determined and applied during impact. The determination of this point utilizes a technique called the Singular Value Decomposition (SVD) Method [50]. However, other methods of finding transformations also exist.

4.4.1 Finding Rotation and Translation of a data set

With the SVD method, the optimal transformation between two sets of corresponding data can be determined (Figure 4.5). In the context of motion tracking, the SVD method can be used to determine the transformation between two different data sets at two instances in time.

If A describes one data set and B describes the same data set at a different time, then the transformation between the two can be expressed in terms of a rotation matrix, $[R]$, and translation vector, t (Equation 4.7). The goal of the SVD method is to find this matrix and vector, $[R]$ and t. These transformations can then be applied
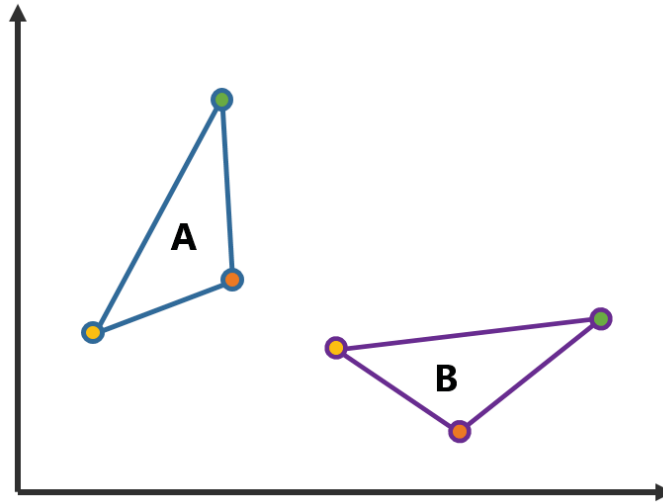
Figure 4.5: Dataset Transformation

Utilizing the SVD method, the rotation and translation between two data sets may be determined

to any other point in data set A to find their corresponding location in data set B. Accordingly, the locations of a point can be found in any instant in time if the initial locations of a data set are known. A and B are each matrices where each column is a vector of coordinates.

$$A = [R] \times B + t \tag{4.7}$$

Finding the rotation and translation matrix with the SVD method can be broken down into three steps:

1. Find the centroids of each data set

2. Find the rotation matrix, $[R]$, between data sets

3. Find the translation vector, t, between data set centroids

In order to find the optimal rotation, the two data sets are overlaid at their centroids to remove any translation. The centroids can be found using equation 4.8.

$$centroid = \frac{1}{N} \sum_{i=1}^{N} P_i \tag{4.8}$$

where

$$N \quad = \quad \text{Number of Points in Dataset}$$

$$P_i \quad = \quad \text{Points in a data set with } x, y, \text{ and } z \text{ components}$$

A covariance matrix, H, can then be created to apply the SVD method (Equation 4.9, 4.10).

$$H = \sum_{i=1}^{N} (P_{A,i} - centroid_A)(P_{B,i} - centroid_B)^T \tag{4.9}$$

$$[U, S, V] = SVD(H) \tag{4.10}$$

where

$$H \quad = \quad \text{Covariance Matrix}$$

$$U, S, V \quad = \quad \text{SVD Decomposition Matrices of the Covariance Matrix}$$

The SVD method decomposes a matrix, such that $H = USV^T$. U and V are square matrices used to determine rotation, while S is a diagonal matrix used to determine scaling. For the application of head-helmet displacement, S is not used. Polar decomposition can then be used to calculate the rotation matrix and translation vectors using Equations 4.11 and 4.12 respectively.

$$[R] = [V][U]^T \tag{4.11}$$

$$t = -[R] \times centroid_A + centroid_B \qquad (4.12)$$

With the rotation and translation matrix, R and t, equation 4.7 can be applied to any data point in data set A. The location of a point in data set A can then be found at a different instance of time, corresponding with dataset B (Figure 4.6). In the context of indirect motion tracking, an initial reference image was taken to be data set A. This reference image contains at least 4 points; three of these points are tracked directly and the last point is tracked indirectly. The rotation and translation of the three points is found between this reference image and any frames of a video. The rotation and translation can then be applied to the 4th indirectly tracked point to determine the location of the 4th point in all frames of a video.
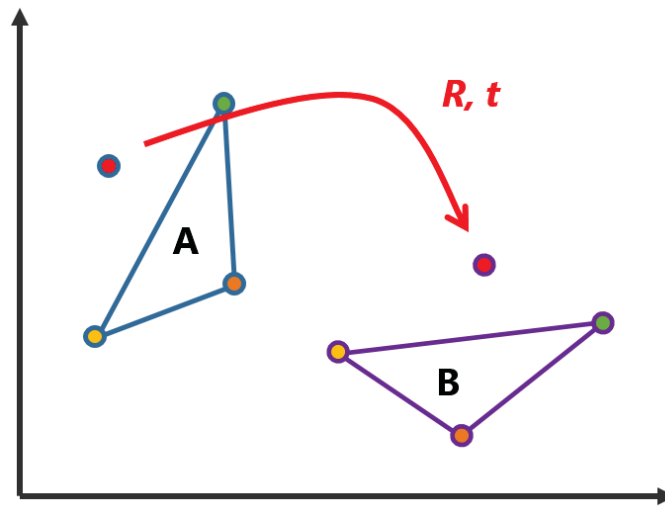
Figure 4.6: Application of Rotation and Translation Matrices

R and t represent the rotation and translation between two data sets

In finding the optimal rotation between data sets A and B, at least three points must be included in the data set. Using a method of least squares, more points can be included and accuracy can be improved.

4.4.2 Accuracy of Indirect Point Tracking

In order to evaluate the accuracy of indirect point tracking utilizing the SVD method, a simple accuracy analysis is performed. Similar to the analysis performed to evaluate the DLT method (Section 4.3.2), the known distance between two points is determined. The same experimental setup is also used. One of these point is directly tracked on the headform while the second point is indirectly tracked. By tracking three other points on the head, the second point can be indirectly tracked. Deviation from the expected difference between the points can then interpreted as the error. Three drops are performed for this analysis (Figure 4.7).
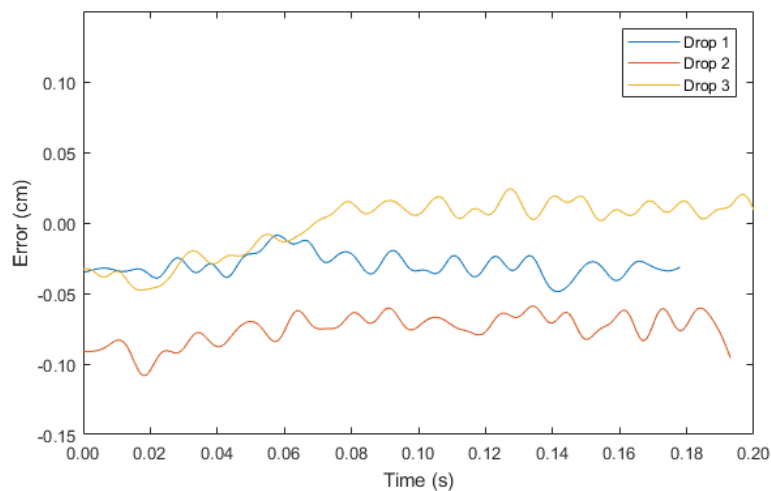
Figure 4.7: Indirect Tracking Error

The error in using the SVD method for indirect tracking was determined for 3 helmeted drops. Each line represents a different drop.

The magnitude of these errors are similar to the DLT method and vary from approximately -0.10 cm to +.05 cm. From the magnitude of these errors, it is accepted that this method is able to achieve a satisfactory accuracy. An error on the scale of millimeters would be sufficient in distinguishing head-helmet displacements on the magnitude of several centimeters.

4.5   Application of Head-Helmet Displacement Tracking

To evaluate head-helmet displacement, a point on the forehead and helmet brim must be tracked during impact. These points are indirectly tracked by tracking 3 points on each the headform and helmet respectively. With the DLT method, the coordinates of these points in 3-D space are determined. A method of indirect tracking is used to track the forehead and helmet brim points specifically. A method has been developed to track head-helmet displacement using a dual high-speed camera setup (Phantom v611) arranged around the drop tower (Figure 4.2). PCC software was again used to determine the 2-D coordinates of markers.

The overall determination of head-helmet displacement may be broken down into 5 steps:

1. Calibrate Space with Calibration Frame

2. Take Head and Helmet References Images

3. Perform Drop

4. Post Process with DLT and Indirect Tracking

5. Calculate Head-Helmet Displacement

The same calibration cage is used (Figure 4.3) to calibrate the space for the DLT method. In order to indirectly track the head and helmet, reference images must also be taken prior to impact (Figures 4.8 and 4.9). These reference images must include the point of interest, as well as 3 points that will be tracked during impact. The point of interest must be visible in the reference only. The 3 tracked markers must be visible in both the reference and in the video of the impact.

Accordingly, three points on each the headform and helmet are tracked during impact (Figure 4.10). The DLT method is applied to find the 3-D coordinates of
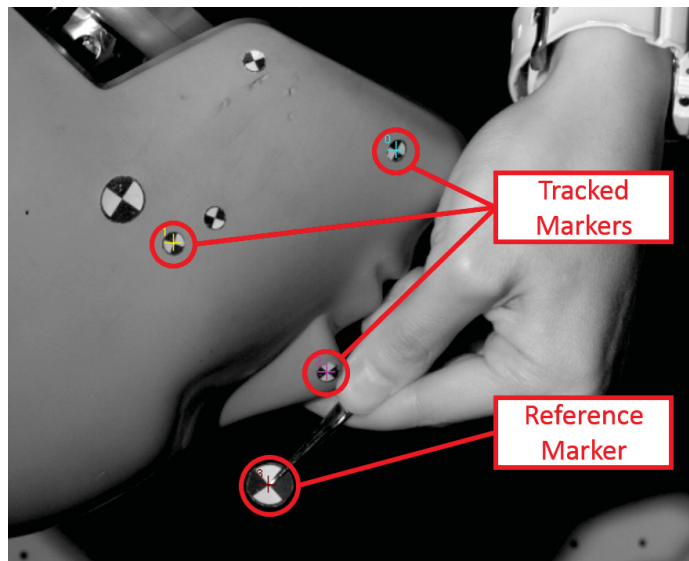
Figure 4.8: Head Reference Image Markers for Motion Tracking

For the head reference, three markers on the head are set as tracked markers and one marker is a reference marker. Copyright Journal of Visualized Experiments. Yu, H., Knowles, B., and Dennison, C.. A test bed to examine helmet fit and retention and biomechanical measures of head and neck injury in simulated impact.
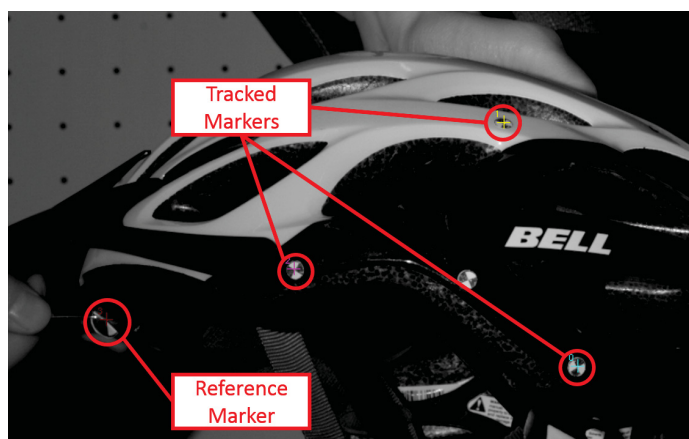
Figure 4.9: Helmet Reference Image Markers for Motion Tracking

For the helmet reference, three markers on the helmet are set as tracked markers and one marker is a reference marker. Copyright Journal of Visualized Experiments. Yu, H., Knowles, B., and Dennison, C.. A test bed to examine helmet fit and retention and biomechanical measures of head and neck injury in simulated impact.

markers. The method of indirect tracking can then be applied to determine the position of the forehead and helmet brim throughout impacts. Finally, the distance between these two points is taken as the head-helmet displacement.
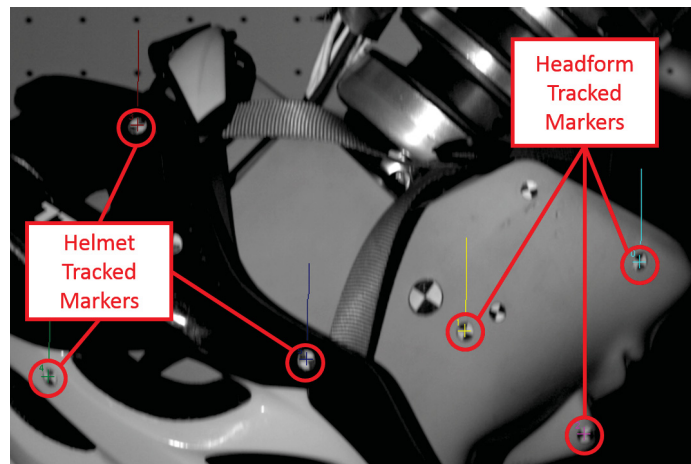
Figure 4.10: Markers Tracked during a Drop

During a drop three markers on each the head and helmet are tracked throughout impact. Copyright Journal of Visualized Experiments. Yu, H., Knowles, B., and Dennison, C.. A test bed to examine helmet fit and retention and biomechanical measures of head and neck injury in simulated impact.

An example of this method of measuring head-helmet displacement during an impact is shown in figure 4.11. The absolute value of the distance between forehead and helmet brim is measured, represented as "Absolute Displacement". This measure most directly compares with HPI. If a helmet is positioned far backwards on the head, absolute head-helmet displacement is expressed as a larger number. At 0 ms, the non-zero displacement represents the position of the helmet prior to impact. At 50 ms, an increase in head-helmet displacement may be observed. This increase corresponds to the helmet's movement as a result of the impact. From this plot, two values are reported: peak absolute displacement and maximum relative change in displacement. Peak absolute displacement is the largest value while maximum relative change is the difference between the largest and smallest values of absolute displacement. In this impact, the peak absolute displacement and relative change in displacement are 19.93 cm and 12.18 cm respectively. Peak absolute displacement aims to describe

the maximum amount of head exposure while relative change aims to describe the helmet's movement during an impact. Higher peak absolute displacements would convey larger head exposures while higher relative change in displacements convey more helmet movement.
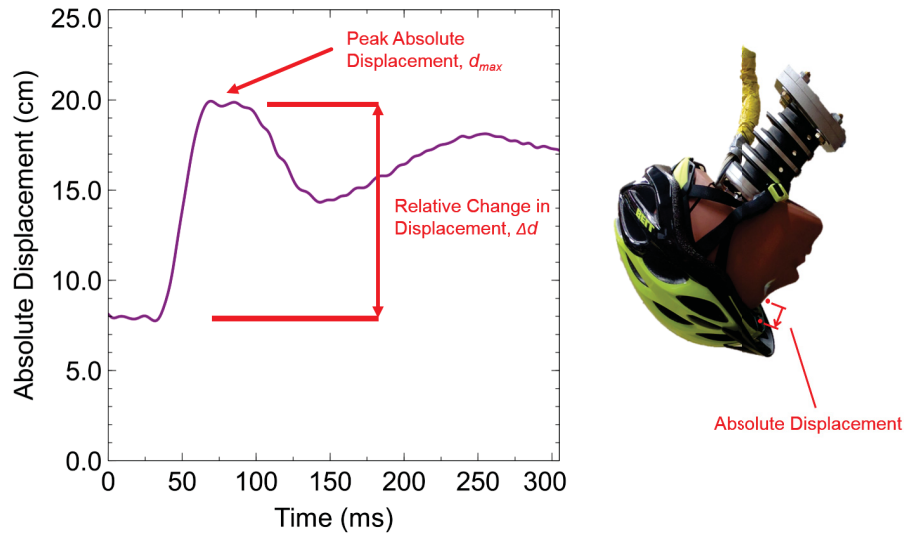
Figure 4.11: Head Helmet Displacement for a Backward Fit Helmet in Impact

Relative change in displacement is also indicated. The vector for absolute displacement is also shown on the right. The absolute displacement begins at around 8 cm, representing the initial helmet position in the backward fit scenario.

4.6 Method Discussion

This method of tracking helmet movement allows absolute and relative head-helmet displacement to be determined. Absolute displacement conveys the amount of facial and forehead exposure during impact while relative displacement conveys retention ability and stability of the helmet. If a helmet excessively exposes the head, represented through a large peak absolute displacement, the helmet may be deemed to insufficiently protect a head throughout impact. With peak absolute displacements, the source of displacements may be a combination of initial helmet position and helmet retention ability. In addition to facial exposure, it may also be valuable to be able to independently assess the helmet's retention ability. A relative change in displacement

can express a helmet's retention ability regardless of initial helmet position. In scenarios where high absolute displacements are observed, it may be beneficial to know if the high displacements are a result of poor initial helmet positioning or poor retention ability. Determining relative change in displacements demonstrate the role of helmet retention. From the accuracy analyses, sub-centimeter accuracy of this method is shown to be possible. This accuracy is acceptable because experimental repeatability would create more variation in helmet displacements. Furthermore, deviations on the scale of millimeters would be relatively negligible in describing head exposure. Both of these measures can be valuable in capably assessing helmet performance .

In the proposed method, a simple vector between helmet brim and forehead was defined as head-helmet displacement. However, the same experimental methods are also able to measure displacement in three component directions (i.e. x, y, and z). Added components could more thoroughly characterize helmet movement and reveal the specific directions of helmet movement. Rotational components could be included also to indicate the amount of rotation of the helmet. These additional components could be particularly valuable, especially in the case of other impact conditions such as a side impact. For simplicity, only a single component was used to express displacement. This single component also provides the closest comparison to HPI for simple interpretation.

Currently, no methods exist to quantitatively characterize helmet movement during an impact. The proposed methods of tracking helmet movement are the first of their kind, and can offer valuable insight on helmet stability and protective efficacy. In the context of evaluating the effect of helmet fit, this method will be particularly valuable in assessing helmet movement.

These methods for characterizing helmet movement could be extended in studies beyond helmet fit. For instance, there has been recent developments of helmet technology aiming to decouple the head from the helmet during impact. This decoupling

would theoretically reduce rotational forces imparted to the head and reduce brain injury likelihood. With the ability to observe helmet movement during impact, better understanding of the head-helmet interaction could be achieved and the effectiveness of the technology could be verified. Tracking head-helmet displacement could provide insight in any situation where helmet movement, stability, or retention is of interest.

CHAPTER 5

EFFECTS OF HELMET FIT ON BIOMECHANICAL PARAMETERS OF HEAD AND NECK INJURY

The effect of helmet fit on injury indicated by biomechanical injury assessment parameters is investigated by simulating different fit scenarios in different impact configurations. Alongside determining biomechanical measures of head and neck injury, newly developed methods of fit force measurement described in Chapter 3 and helmet movement tracking described in Chapter 4 are also implemented.

5.1 Background

Poor helmet fit is associated with lesser helmet protective performance in select epidemiological studies [5, 6, 7] and intuitively a helmet should perform most optimally when used as designed. Better understanding of the mechanics associated with head and neck injury risk associated with improper helmet use could lead to unambiguous conclusions concerning the importance of helmet fit. Different fit scenarios are investigated under the simulation of different impact scenarios utilizing a test bed used to study biomechanical measures of head and neck injury. The previously developed methods of quantifying fit forces and measuring head-helmet displacement are also implemented to further analysis [51]. In Chapter 3, the development and application

of a fit sensor using FBGs was described. All the fit force measurement components of this study were previously carried out and also described in Chapter 3, Section 3.3. In Chapter 4, the development of a method of tracking helmet movement relative to the head using a dual high speed camera setup is described. By comparing different measures of injury risk in different fit scenarios, the importance of correct helmet fit can be understood.

5.2 Materials and Methods

Details of the experimental methods are described in the peer reviewed journal publication:

Henry Y. Yu, Brooklynn M. Knowles, and Christopher R. Dennison. A test bed to examine helmet fit and retention and biomechanical measures of head and neck injury in simulated impact. *Journal of Visualized Experiments*, 2017. (In Press)

5.2.1 Experimental Equipment

For impact simulation, a custom designed linear impact tower is used to guide an ATD during freefall onto a steel anvil. The impact tower consists of an adjustable drop gimbal, a Hybrid III 50th Percentile head and neck, and variable impact surface. 9 uni-axial accelerometers (Measurement Specialties Inc. Hampton VA, model 64C-2000-360) arranged in a 3-2-2-2 configuration within the head allow linear and angular accelerations of the headform to be determined at the center of gravity. A six-axis upper neck load cell is also included to measure forces and moments at a location approximately corresponding to the human spine OC vertebrae. A purpose built velocity gate is also arranged on the impact tower to measure impact velocity immediately before impact. A National Instruments data acquisition system (PXI 6251 with LabVIEW v.8.5, Austin TX) was used to collect head acceleration and

neck force/moment data. Prior to the data acquisition system, signals are filtered with a hardware anti-aliasing filter with a corner frequency of 4 kHz. The signals are then sampled at a frequency of 100 kHz for all channels. After data collection, data is further processed with MATLAB through a low-pass filter. These sampling and filtering meet industry recommended practices for use of Hybrid III anthropometric test devices [52].

Two Phantom v611 cameras (Vision Research, Wayne NJ) were arranged around the drop tower to capture stereoscopic movements between the headform and helmet. A master camera was placed to the side of the drop tower while a slave camera was placed at approximately 45° from the master. A 250 W light was also setup between the cameras to allow for sufficient exposure. Each camera was equipped with either a Carl Zeiss (Jena, Germany) 50 mm f/1.4 or Carl Zeiss 100 mm f/2.0 macro lens, depending on the field of view required. The apertures on the lenses were set at f/8.0. This aperture was chosen to allow for sufficiently sharp focus in the desired depth of field. The required field of view ranged from 30 cm to 60 cm, depending on the impact scenario. The cameras were both configured to record at 1280 x 800 pixels at a frame rate of 1000 frames per second or faster. The exposure time per frame was at most 600 μsec. The two-dimensional coordinates of each marker is found with tracking software (Phantom Camera Control 2.6, Vision Research, Wayne NJ). The overall experimental setup is shown in Figure 5.1.

A CPSC certified helmet (Traverse, Bell, Rantoul, IL), available in both Universal and Extra Large sizes, was chosen for all four fit scenarios. This helmet was chosen because of its typical construction and design for a commuter cycling helmet. The four fit scenarios consist of an normal, oversized, forward, and backward fit. An oversized helmet uses an extra large helmet, while all other fit scenarios use a universal size. The forward and backward fit correspond to different helmet positioning, shown in Figure 5.2. Fit scenario definition and choice is detailed in Section 3.3.
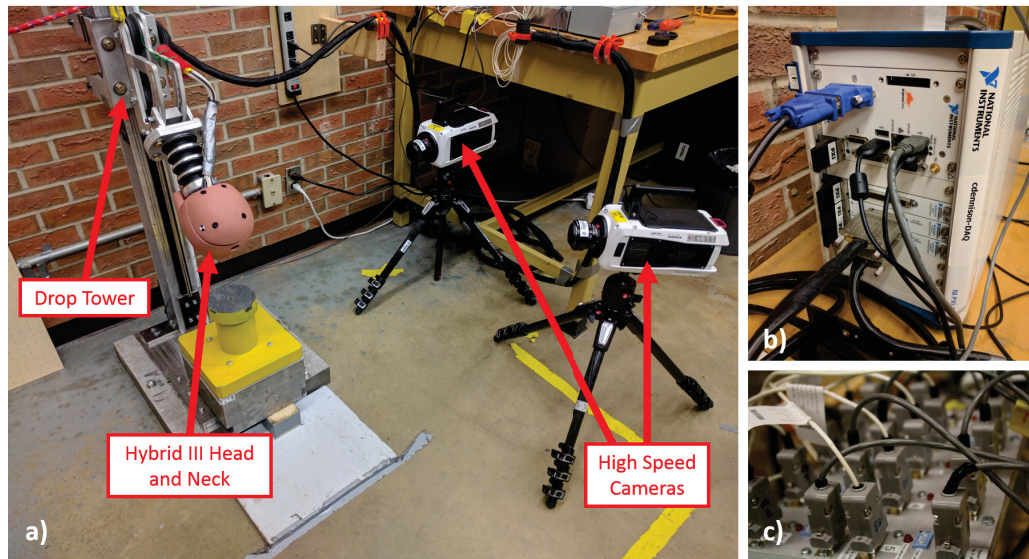
Figure 5.1: Overall Experimental Setup

The overall experimental setup is shown, consisting of a drop tower with a Hybrid III head and neck surrounded by two high speed cameras (a). Signals from the Hybrid III are sampled by a National Instruments DAQ (b) after being amplified and going through a hardware anti-aliasing filter (c)
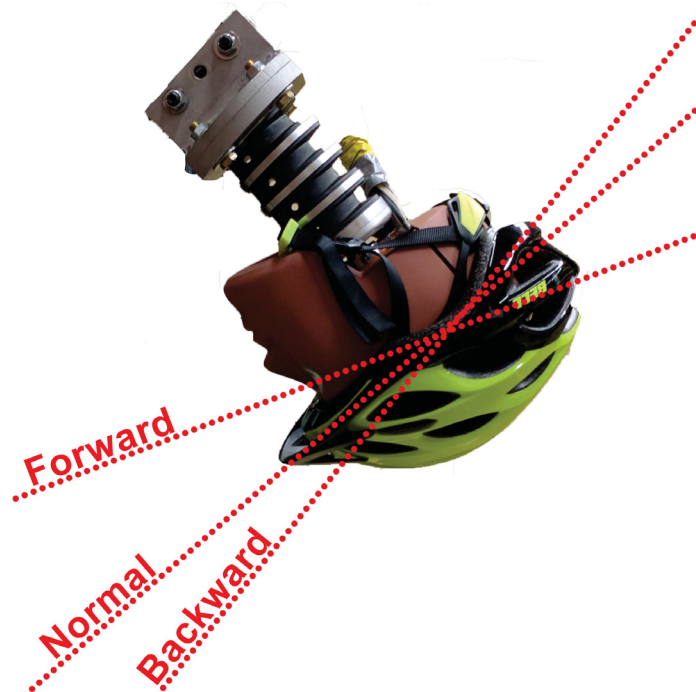
Figure 5.2: Helmet Positioning Fit Scenarios

A forward and backward helmet fit scenario are shown relative to a normal fit

5.2.2 Experimental Procedure

Four fit scenarios were studied, varying the sizing and position of the helmet. According to manufacturer provided fit guide based on circumference, a universal size most appropriately fits the Hybrid III headform circumference of 575 mm. These fit scenarios are the same as described in Chapter 3: Normal, Oversized, Forward, and Backward fit (Table 3.2).

Fit force measurement was previously performed, described in Chapter 3, Section 3.3.

All drops were performed to impact the forehead, a common impact location in cycling, although other scenarios could also be simulated. Six different impact scenarios were simulated by varying impact speed, impact surface, and either head-first or torso-first impacts. Two impact velocities of 4 m/s and 6 m/s were chosen based on previous literature and standards. The headform was dropped from an appropriate height to achieve these velocities. One of either a flat or a 45° angled anvil was arranged (Figure 5.3). The flat anvil simulates falls on a flat surface, while the angled anvil simulates impacts with a tangential velocity component. Both the surface of these anvils were covered in abrasive tape to simulate an asphalt surface. Relative to a bare steel surface, the abrasive tape could produce more of a tangential force component during impact. Adjustment of anvil position was occasionally necessary between impacts to ensure the helmet to be impacted would contact the flat of the anvil only. Both head-first and torso-first impacts were simulated, with torso impacts similar to the combined loading impact configuration presented in Smith et al [53]. For torso first impacts, a wooden block was placed in the path of the drop gimbal to simulate the torso hitting the ground before the head. The positioning of the the block was arranged at a height such that neck flexion would begin with the head approximately 25 mm above the anvil. This neck flexion would then allow the head

to impact the anvil. A layer of foam was also included above the wooden block to minimize vibrations from the drop tower at torso impact. It is recognized that different configurations of the neck angle and positioning of the wooden block could produce a variety of different impact parameters. The chosen configuration is one of many configurations, and is not necessarily representative of all torso impacts which may vary in amounts of neck flexion or timings between torso and head impacts.
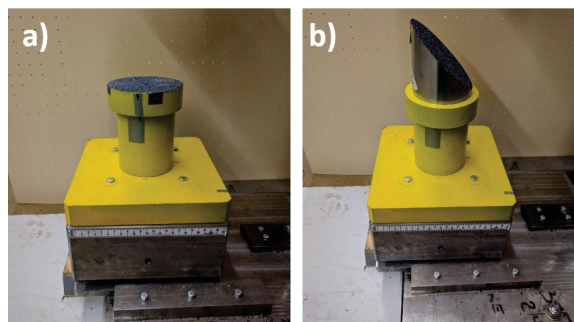
Figure 5.3: a) Flat and b) Angled Anvil

Copyright Journal of Visualized Experiments. Yu, H., Knowles, B., and Dennison, C.. A test bed to examine helmet fit and retention and biomechanical measures of head and neck injury in simulated impact.

Table 5.1: Simulated Impact Scenarios

Impact Speed	Impact Surface	Head/Torso First
Low (4 m/s)	Flat	Head
High (6 m/s)	Flat	Head
Low	Angled	Head
High	Angled	Head
Low	Flat	Torso
High	Flat	Torso

Each of the four fit scenarios were subject to each of the 6 impact scenarios. After 3 trials of each configuration a total of 72 drops were performed, each drop using a new helmet.

Following data collection, code was processed through MATLAB to meet J211 recommended practice. Head accelerations and neck forces were filtered with a 4th order Butterworth filter with a corner frequency of 1,650 Hz. A similar filter was

utilized for neck moment signals, but with a corner frequency of 1,000 Hz. With the measured linear accelerations, angular accelerations could also be determined [54].

For this study, the following metrics were calculated and reported:

- Peak Linear Acceleration, Peak g

- Peak Angular Acceleration, Peak α

- Peak Angular Velocity, Peak ω

- Change in Angular Velocity, $\Delta\omega$

- Cumulative Strange Damage Measure, CSDM

- Maximum Principle Strain, MPS

- Peak Neck Injury Criterion, N_{ij}

- Peak Head-Helmet Displacement, d_{max}

- Relative Change in Displacement, Δd

Linear acceleration is the main method of quantifying the severity of head impacts to characterize focal injury and it is used in virtually all helmet standards as a pass/fail criterion [10, 55]. Accordingly, Peak g was measured for all impacts. As angular kinematics have been shown to be a better predictor for diffuse brain injuries [25], α, ω, and $\Delta\omega$ were also measured.

Evaluating likelihood of brain injury also included the use of a brain finite element model. One model was developed by Takhounts, called the Simulated injury Monitor (SIMon) [25], which is available online through the National Highway Traffic Safety Administration and is used in this thesis. By using head kinematics as input for the model, strains in the brain may be determined. More strain in the brain would then correlate with more damage in brain tissue, which presumably results in more brain injury. This finite element model approximates the geometry, anatomy, and mechanical properties of an average male head, including the skull, cerebrospinal fluid layers,

bridging veins, and brain. The model is capable of finding cumulative strain damage measure (CSDM), the volume fraction of the brain reaching a certain strain threshold, and maximum principal strain (MPS). These strain measures were established to correlate well with angular head kinematics, which biomechanical research suggests capably predicts diffuse injury [25]. The human finite element head model was also tuned and validated with cadaveric and animal brain injury experiments [28]. Although SIMon was developed for automotive injury assessment, it was validated to give realistic brain tissue deformation in impact of similar severity and time duration to helmeted impacts and its injury assessment metrics were developed using both automotive and sports injury data. The use of SIMon has also been extensively used in the Biomedical Instrumentation Lab for investigating brain strains [56, 57, 46].

Neck forces and moments were also measured, which were then used to compute neck injury criterion N_{ij}. With N_{ij}, axial and bending moments are combined and normalized with critical limits of the neck.

The methods used for determining head-helmet displacement are developed in Chapter 4, with the experimental equipment and procedure detailed in Section 4.5. Peak Head-Helmet Displacement, d_{max}, is used to characterize the amount of head exposure while relative change in displacement, Δd is used to character helmet movement.

Calculation of the metrics are detailed in Appendix A.

A two-tailed t-test was then used to compare the means of each metric between different fit scenarios. Each the oversized, forward, and backward fits were compared to a normal fit scenario. A significance of p <0.005 was chosen.

5.3 Results

Summary of the head kinematics and finite element model strains is reported in Table 5.2. A summary of neck kinetics and Nij is reported in Table 5.3. Finally, head-helmet displacement results are summarized in Table 5.4. Again, fit force measurements results are described in Chapter 3. For all kinematics, results were reported as peak resultant values of each the x, y, and z components so that reported kinematics may be compared with other work. Biomechanical measures for injury risk are often based on resultant kinematics.

5.3.1 Head Kinematics

Typical transient linear acceleration plots for two different impact scenarios are shown in Figure 5.4. In head-first impacts, the poor fit scenarios exhibited lower peak g's during impact. These lower peak linear acceleration values suggest that risk of focal injury may be lower in the scenarios of poor helmet fit, when compared to a properly fit helmet. The greatest significance was observed in the impact scenario at 6 m/s, on a flat anvil, and head-first. A normally fit helmet experienced a peak g of 161.7 ± 2.7 g, while a oversized, forward, and backward helmet experienced a peak g of 145.6 ± 1.1 g, 127.0 ± 2.3 g, and 125.7 ± 0.6 g, respectively (Table 5.2). Impacts on an angled anvil at 6 m/s showed similar results, but of a lower magnitude. Of these angled impacts, only a backward fit scenario at high impact speed was significantly different than a properly fit helmet. Torso first impacts did not show a similar trend and did not have any fit scenarios show significantly different peak g values compared to a normally fit helmet.

Typical angular acceleration and angular velocity plots for two different impact scenarios are shown in Figure 5.5 and 5.6, respectively. Based on angular acceleration, angular velocity, CSDM, and MPS, the effect of poor helmet fit on brain injury

likelihood in impact is not increased in all cases. In either head first or torso first scenarios, no impacts showed significant differences in angular velocity. For head first impacts, CSDM and MPS showed similarly unvaried results between different fit scenarios, except in one impact scenario. In this low speed head-first impact onto an angled anvil, an oversized helmet was shown to have statistically significantly higher CSDM and MPS. However, the differences are small and not practically significant due to small increase in injury risk.

In torso first impacts, the backward fit scenario showed potential increases in each angular acceleration, angular velocity, CSDM, and MPS. For a 6 m/s torso first impact, a normally fit helmet and backward fit helmet experienced a CSDM of 0.51 ± 0.01 and 0.78 ± 0.05, respectively. A t-test showed that this difference is significant. Similarly for the normally fit and backward fit scenarios, there were peak angular velocities of 26.13 ± 3.28 rad/s and 41.24 ± 6.47 rad/s, respectively, with a p-value of 0.023. This p-value is near significance and the difference in means is relatively large. This result in angular acceleration is consistent with CSDM, which further reinforces that a backward fit scenario may be associated with an increased likelihood of brain injury. At a lower speed (4 m/s) the oversized and forward fit scenarios were shown to have significantly lower CSDM values. The lower CSDM values suggests that the oversized and forward fit scenarios may result in a lower risk of brain injury for this type of impact.

Overall, impacts to an angled anvil were able to show higher angular kinematics and lower linear kinematics when compared to impacts to a flat anvil.
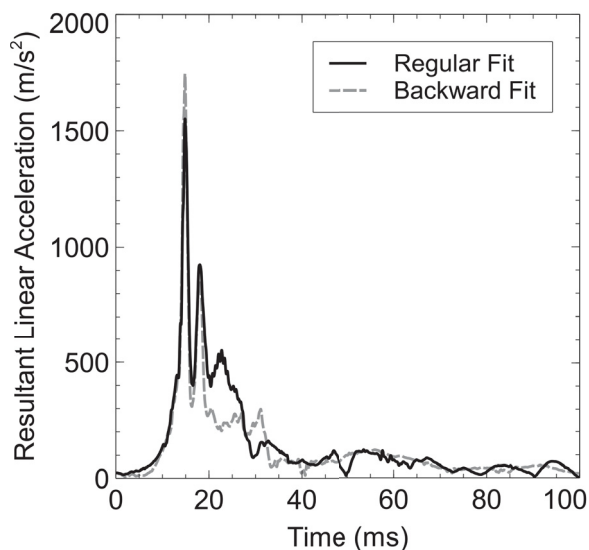
Figure 5.4: Resultant Head COG (Center of Gravity) Linear Acceleration

Resultant head center of gravity (COG) linear acceleration for a torso first-impact onto a flat anvil at 6 m/s. A regular fit and backward fit scenario are compared. Copyright Journal of Visualized Experiments. Yu, H., Knowles, B., and Dennison, C.. A test bed to examine helmet fit and retention and biomechanical measures of head and neck injury in simulated impact.
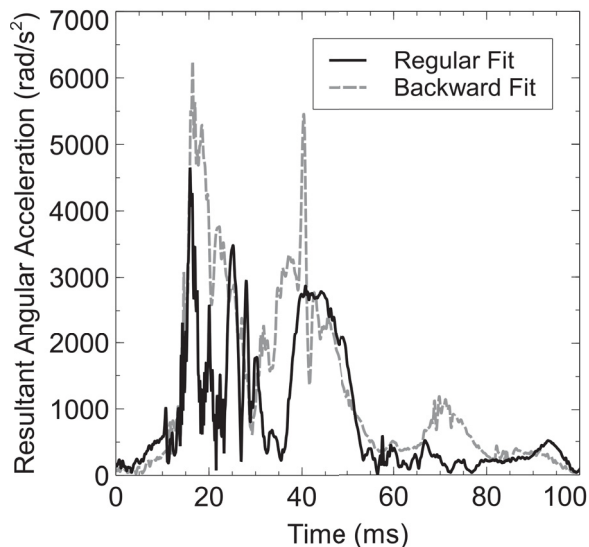
Figure 5.5: Resultant Head COG (Center of Gravity) Angular Acceleration

Resultant head center of gravity (COG) angular acceleration for a torso first-impact onto a flat anvil at 6 m/s. A regular fit and backward fit scenario are compared. Copyright Journal of Visualized Experiments. Yu, H., Knowles, B., and Dennison, C.. A test bed to examine helmet fit and retention and biomechanical measures of head and neck injury in simulated impact.
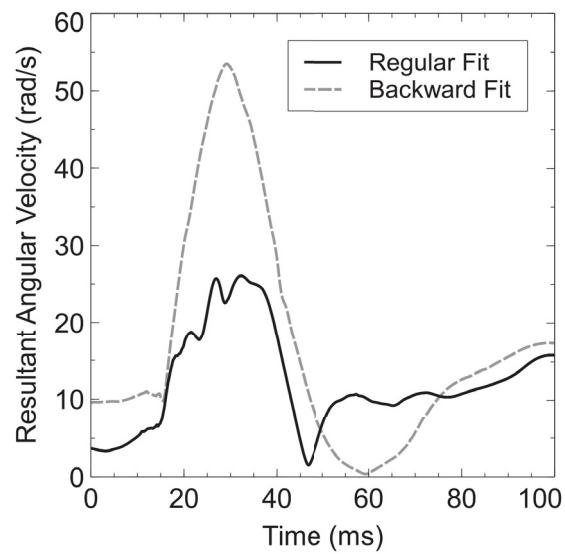
Figure 5.6: Resultant Head COG (Center of Gravity) Angular Velocity

Resultant head center of gravity (COG) angular velocity for a torso first-impact onto a flat anvil at 6 m/s. A regular fit and backward fit scenario are compared. Copyright Journal of Visualized Experiments. Yu, H., Knowles, B., and Dennison, C.. A test bed to examine helmet fit and retention and biomechanical measures of head and neck injury in simulated impact.

Table 5.2: Head Kinematic Results

(a) Flat Anvil, Head First

Fit Scenario	Peak g (g)	p-value	Peak α (rad/s²)	p-value	Peak ω (rad/s)	p-value	Δω (rad/s)	p-value	CSDM15	p-value	MPS	p-value
Low Speed (4 m/s)												
Normal	87.2 ± 2.9	-	3178.9 ± 167.7	-	18.5 ± 3.5	-	17.4 ± 2.7	-	0.14 ± 0.07	-	0.01 ± 0.00	-
Oversized	86.8 ± 2.3	0.842	5270.6 ± 253.9	0.000	18.7 ± 3.0	0.939	16.6 ± 4.1	0.794	0.16 ± 0.02	0.617	0.03 ± 0.03	0.801
Forward	80.0 ± 4.1	0.067	3098.4 ± 264.6	0.679	19.1 ± 1.6	0.791	18.8 ± 1.5	0.474	0.17 ± 0.01	0.540	0.01 ± 0.00	0.583
Backward	76.3 ± 3.8	0.016	3626.9 ± 164.4	0.030	16.5 ± 1.8	0.427	15.4 ± 1.8	0.350	0.11 ± 0.03	0.511	0.00 ± 0.00	0.517
High Speed (6 m/s)												
Normal	161.7 ± 2.7	-	5229.1 ± 156.6	-	26.5 ± 1.1	-	25.7 ± 0.9	-	0.22 ± 0.03	-	0.01 ± 0.00	-
Oversized	145.6 ± 1.1	0.001	6017.7 ± 722.7	0.138	26.5 ± 4.6	0.998	24.4 ± 2.0	0.362	0.19 ± 0.08	0.637	0.01 ± 0.01	0.828
Forward	127.0 ± 2.3	0.000	4411.4 ± 322.7	0.017	24.4 ± 7.7	0.664	21.1 ± 8.0	0.377	0.20 ± 0.06	0.657	0.01 ± 0.01	0.631
Backward	125.7 ± 0.6	0.000	5511.0 ± 648.2	0.505	28.9 ± 2.7	0.224	27.0 ± 3.2	0.557	0.24 ± 0.07	0.593	0.02 ± 0.01	0.407

(b) Angled Anvil, Head First

Fit Scenario	Peak g (g)	p-value	Peak α (rad/s²)	p-value	Peak ω (rad/s)	p-value	Δω (rad/s)	p-value	CSDM15	p-value	MPS	p-value
Low Speed												
Normal	62.7 ± 4.9	-	8446.5 ± 733.8	-	22.2 ± 1.9	-	21.3 ± 1.1	-	0.13 ± 0.01	-	0.01 ± 0.00	-
Oversized	65.0 ± 0.6	0.471	7754.7 ± 341.1	0.213	22.1 ± 1.9	0.921	21.3 ± 2.1	0.989	0.17 ± 0.01	0.004	0.01 ± 0.00	0.003
Forward	46.7 ± 1.3	0.006	6292.9 ± 365.1	0.010	22.1 ± 1.1	0.910	21.8 ± 1.4	0.655	0.15 ± 0.01	0.125	0.01 ± 0.00	0.416
Backward	43.7 ± 5.2	0.010	7551.4 ± 647.2	0.188	21.9 ± 1.5	0.822	21.6 ± 1.6	0.823	0.13 ± 0.00	0.582	0.01 ± 0.00	0.671
High Speed												
Normal	91.8 ± 5.8	-	12607.3 ± 461.7	-	32.8 ± 2.6	-	31.6 ± 3.3	-	0.49 ± 0.02	-	0.11 ± 0.00	-
Oversized	80.7 ± 4.2	0.054	11218.7 ± 274.9	0.011	36.9 ± 1.8	0.093	36.0 ± 2.3	0.134	0.54 ± 0.02	0.021	0.13 ± 0.02	0.265
Forward	80.7 ± 4.7	0.060	9541.3 ± 750.5	0.004	35.7 ± 4.4	0.387	34.1 ± 4.1	0.458	0.52 ± 0.11	0.680	0.11 ± 0.03	0.320
Backward	61.1 ± 2.5	0.001	10624.7 ± 1149.8	0.050	34.9 ± 4.8	0.546	33.9 ± 3.9	0.476	0.54 ± 0.08	0.313	0.12 ± 0.03	0.254

(c) Flat Anvil, Torso First

Fit Scenario	Peak g (g)	p-value	Peak α (rad/s²)	p-value	Peak ω (rad/s)	p-value	Δω (rad/s)	p-value	CSDM15	p-value	MPS	p-value
Low Speed												
Normal	52.7 ± 2.8	-	3426.4 ± 108.6	-	31.3 ± 3.2	-	30.2 ± 4.4	-	0.55 ± 0.06	-	0.09 ± 0.02	-
Oversized	59.1 ± 5.9	0.167	3993.3 ± 1078.5	0.051	26.1 ± 0.7	0.416	25.8 ± 0.9	0.162	0.27 ± 0.04	0.002	0.02 ± 0.01	0.017
Forward	61.4 ± 11.6	0.280	4941.1 ± 1213.1	0.107	27.0 ± 1.8	0.098	26.5 ± 1.5	0.243	0.31 ± 0.04	0.004	0.03 ± 0.01	0.016
Backward	63.5 ± 3.7	0.015	3575.8 ± 98.6	0.245	33.8 ± 0.5	0.152	33.4 ± 0.5	0.279	0.64 ± 0.00	0.053	0.13 ± 0.00	0.133
High Speed												
Normal	164.3 ± 5.8	-	4752.3 ± 127.4	-	26.1 ± 3.3	-	23.5 ± 1.7	-	0.51 ± 0.01	-	0.09 ± 0.01	-
Oversized	175.8 ± 17.5	0.343	4259.0 ± 116.8	0.008	21.4 ± 1.3	0.080	21.0 ± 1.3	0.111	0.50 ± 0.06	0.813	0.10 ± 0.02	0.877
Forward	182.0 ± 1.5	0.007	7588.9 ± 6521.1	0.493	21.8 ± 1.1	0.099	21.1 ± 0.9	0.109	0.53 ± 0.01	0.168	0.11 ± 0.01	0.184
Backward	179.7 ± 1.5	0.011	5754.1 ± 699.1	0.071	41.2 ± 6.5	0.023	39.7 ± 5.0	0.006	0.78 ± 0.05	0.001	0.27 ± 0.06	0.007

P-values of 0.000 only reflect a significance level lower than the shown levels of precision, not zero. Shaded cells indicate significance of $p < 0.005$.

5.3.2   Neck Kinetics

Typical transient plots for resultant neck force and neck moment are shown in Figures 5.7 and 5.8 respectively. Nij was also computed, shown in Figure 5.9. The results comparing Nij (Table 5.3) did not suggest any significant differences in likelihood for neck injury between a poor and properly fit helmet scenario. Between all impact scenarios, changes in neck injury criterion were not statistically significant. Even the scenarios close to significance showed relatively small differences, suggesting minimal practical significance. The largest values of Nij were noted in the high speed head-first impact scenario, reaching values of 1.74. The highest values of Nij, which were only found in the high speed head-first impacts, corresponds to approximately a 55% chance of AIS 3 injury [23]. AIS 3 neck injuries are considered "serious" and include vertebrae fracture, spinal cord contusion/compression [58]. However, the trends in neck injury likelihood, should again be the focus.
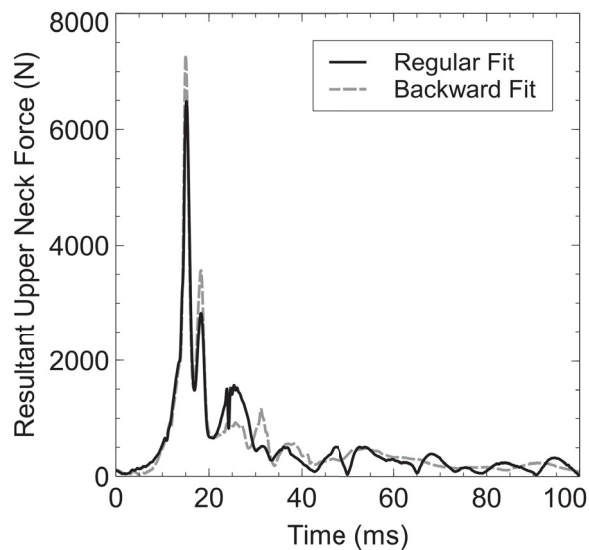
Figure 5.7: Resultant Neck Force

Resultant neck force for a torso first-impact onto a flat anvil at 6 m/s. A regular fit and backward fit scenario are compared. Copyright Journal of Visualized Experiments. Yu, H., Knowles, B., and Dennison, C.. A test bed to examine helmet fit and retention and biomechanical measures of head and neck injury in simulated impact.
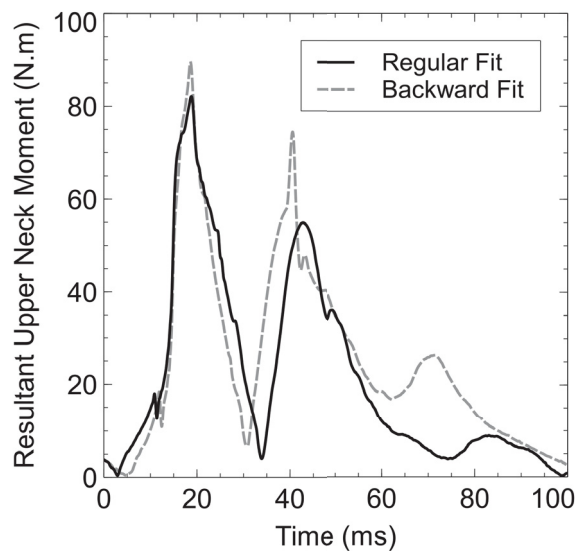
Figure 5.8: Resultant Neck Moments

Resultant neck moment for a torso first-impact onto a flat anvil at 6 m/s. A regular fit and backward fit scenario are compared. Copyright Journal of Visualized Experiments. Yu, H., Knowles, B., and Dennison, C.. A test bed to examine helmet fit and retention and biomechanical measures of head and neck injury in simulated impact.
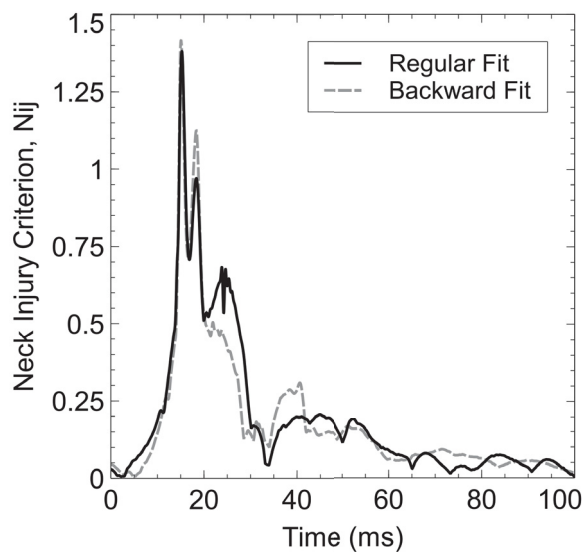
Figure 5.9: Resultant Neck Injury Criterion

Nij for a torso first-impact onto a flat anvil at 6 m/s. A regular fit and backward fit scenario are compared. Copyright Journal of Visualized Experiments. Yu, H., Knowles, B., and Dennison, C.. A test bed to examine helmet fit and retention and biomechanical measures of head and neck injury in simulated impact.

Table 5.3: Neck Kinetic Results

(a) Flat Anvil, Head First

Fit Scenario	Nij	p-value
Low Speed (4 m/s)		
Normal	1.22 ± 0.12	-
Oversized	1.05 ± 0.03	0.073
Forward	1.12 ± 0.02	0.217
Backward	1.11 ± 0.11	0.318
High Speed (6 m/s)		
Normal	1.74 ± 0.07	-
Oversized	1.66 ± 0.06	0.174
Forward	1.68 ± 0.05	0.223
Backward	1.72 ± 0.04	0.626

(b) Angled Anvil, Head First

Fit Scenario	Nij	p-value
Low Speed		
Normal	0.77 ± 0.03	-
Oversized	0.78 ± 0.01	0.522
Forward	0.77 ± 0.00	0.947
Backward	0.70 ± 0.00	0.019
High Speed		
Normal	1.04 ± 0.01	-
Oversized	1.06 ± 0.02	0.284
Forward	1.08 ± 0.01	0.008
Backward	1.07 ± 0.02	0.223

(c) Flat Anvil, Torso First

Fit Scenario	Nij	p-value
Low Speed		
Normal	0.52 ± 0.02	-
Oversized	0.60 ± 0.11	0.277
Forward	0.56 ± 0.09	0.398
Backward	0.59 ± 0.02	0.012
High Speed		
Normal	1.23 ± 0.03	-
Oversized	1.27 ± 0.06	0.366
Forward	1.26 ± 0.03	0.295
Backward	1.28 ± 0.03	0.099

Shaded cells indicate significance of $p < 0.005$.

5.3.3   Helmet Displacement

Although significance is noted in some instances with head-first impacts, the actual changes in head-helmet displacement were not always of practical significance; relative differences in head-helmet displacement that differed on the scale of about 1-2 cm were not considered noteworthy.

Typical transient head-helmet displacement is shown in Figure 5.10. In many impacts, the normal fit scenarios and backwards fit scenarios exposed the forehead the most, indicated by higher max displacement values (Table 5.4). For these fit
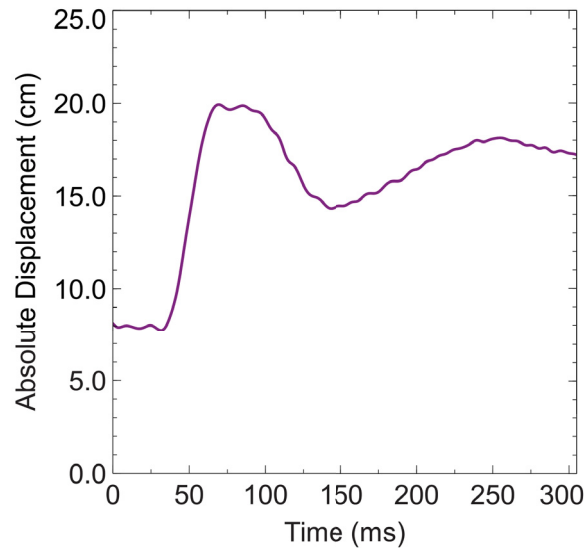
Figure 5.10: Dynamic Head-Helmet Displacements

Head-Helmet Displacement in a torso-first impact onto a flat anvil at 6 m/s for a backward fit scenario. The absolute displacement does not begin at 0 cm due to the initial helmet position. The starting value of approximately 8 cm represents the distance between the helmet brim and forehead, representing the initial helmet position in the backward fit scenario.

scenarios, the most head exposure (maximum head helmet displacement, d_{max}) was observed in torso-first impacts in particular. For a high speed torso first impact, the normal and backward fit scenario reached a maximum displacement of 10.33 ± 0.80 cm and 17.81 ± 1.84 cm, respectively. In contrast, the oversized and forward fit scenarios in the same impact condition reached displacements of 7.09 ± 0.11 cm and 5.72 ± 1.18 cm respectively (Table 5.4).

The relative changes in head-helmet displacement, Δd, suggested that helmet movement was not significantly different between different fit scenarios in head-first or torso-first impacts. Instances of statistical significance were observed in head-first impacts, but with small differences that were not practically significant. One high-speed torso-impact case showed higher relative displacements with near significance. In this torso-first impacts, a backward fit helmet reached a Δd of 10.88 ± 1.13 cm while a normal fit reached 6.98 ± 0.55 cm and a p-value of 0.006.

It should also be noted that head-helmet displacement leading up to impact re-

mained relatively unchanged, as shown in Figure 5.10. The acceleration of the head towards the anvil did not induce noteworthy head-helmet displacements.

Table 5.4: Helmet Displacement Results

(a) Flat Anvil, Head First

Fit Scenario	d_{max}	p-value	Δd	p-value
Low Speed (4 m/s)				
Normal	2.57 ± 0.37	-	1.13 ± 0.09	-
Oversized	1.69 ± 0.11	0.016	1.28 ± 0.14	0.193
Forward	1.07 ± 0.15	0.003	0.60 ± 0.13	0.004
Backward	6.22 ± 0.66	0.001	1.64 ± 0.32	0.059
High Speed (6 m/s)				
Normal	5.21 ± 0.58	-	3.03 ± 0.91	-
Oversized	2.80 ± 0.38	0.004	1.96 ± 0.31	0.127
Forward	1.96 ± 0.59	0.002	1.24 ± 0.56	0.044
Backward	8.74 ± 0.62	0.002	4.41 ± 1.04	0.159

(b) Angled Anvil, Head First

Fit Scenario	d_{max}	p-value	Δd	p-value
Low Speed				
Normal	2.32 ± 0.02	-	0.75 ± 0.03	-
Oversized	1.34 ± 0.07	0.000	0.71 ± 0.06	0.318
Forward	2.84 ± 0.13	0.002	0.45 ± 0.06	0.001
Backward	4.42 ± 1.33	0.052	0.80 ± 0.10	0.483
High Speed				
Normal	1.36 ± 0.09	-	0.28 ± 0.08	-
Oversized	2.30 ± 0.63	0.064	1.02 ± 0.15	0.002
Forward	2.63 ± 0.66	0.030	0.69 ± 0.03	0.001
Backward	4.21 ± 0.59	0.001	0.90 ± 0.32	0.032

(c) Flat Anvil, Torso First

Fit Scenario	d_{max}	p-value	Δd	p-value
Low Speed				
Normal	11.17 ± 1.71	-	8.78 ± 1.64	-
Oversized	7.28 ± 0.92	0.025	5.53 ± 0.45	0.030
Forward	6.81 ± 1.41	0.027	5.04 ± 1.32	0.037
Backward	15.33 ± 0.52	0.016	9.36 ± 0.24	0.582
High Speed				
Normal	10.33 ± 0.80	-	6.98 ± 0.55	-
Oversized	7.09 ± 0.11	0.002	5.19 ± 0.13	0.005
Forward	5.72 ± 1.18	0.005	4.23 ± 0.98	0.013
Backward	17.81 ± 1.84	0.003	10.88 ± 1.13	0.006

P-values of 0.00 only reflect a significance level lower than the shown levels of precision, not zero. Shaded cells indicate significance of p <0.005.

5.4 Discussion

With the different biomechanical metrics, a value can be used to associate different levels of injury. For instance, a peak linear acceleration of 300 g can be associated with skull fracture [10, 55]. However, setting thresholds is controversial. These metrics may

not encompass all the different variables and parameters that may define a scenario. As a result, risk thresholds are not universally agreed upon. As such, any threshold values referenced should then be used to document possible trends in injury risk.

5.4.1 Focal Injury

Considering focal injuries and the peak-g, which is the common kinematic used to assess risk of them, a normal or proper fit was not associated with lesser risk. This finding in our study seems to counter the conventional wisdom but consistent with findings in previous work. In head first impacts, a properly fit helmet did not demonstrate a better ability in preventing focal injury; linear kinematics suggests that risk of focal injury was unchanged between a normally fit helmet and each a oversized, forward, and backward fit scenario.

These linear kinematic results are consistent with related work in investigating helmet fit. In Chang et al's work, different combinations of headform and helmet sizing were simulated in simple impacts onto a flat anvil with a motorcycle helmet. In terms of linear acceleration, the normal fit scenario in their work also performed more poorly than in the scenarios with a mismatch in size [42]. In Klug et al's work, a normal fit was compared to a backward fit in experimental impacts with a cycling helmet. Similar to the findings in this thesis, linear kinematics (HIC) were also found to be lower when compared to a normal fit scenario [44]. Because HIC is shown to vary almost linearly with linear acceleration in different impacts, trends with HIC can be compared to trends in linear acceleration for head impacts [59]. In Jadischke's work with football helmet impacts, peak linear acceleration was also shown to increase with tighter fit [12].

The results of lesser peak g in poor fit scenarios could possibly be explained by two effects dealing with: head-helmet mechanical interaction, and the role of the retention system. Specific to head-helmet mechanical interaction, a potential explanation for

the differences in peak acceleration may be attributed to the variation in contact area between the head and helmet for different fit scenarios. The normal fit should have the most contact between head and helmet, when compared to an oversized, forward, or backward fit scenario. This would allow for the head to endure more force within a shorter amount of time and effectively increase the resultant linear acceleration. Although the load may be better distributed across the head with a properly fit helmet, the global force experienced by the head may be greater. Another potential mechanism is the transfer of energy to the retention system. In a poorly fit helmet, the retention system could be taking more of the load during impact. Helmet displacement results may also further support this claim, as the relative changes in displacements (Δd) in cases of significance are low. Because the retention system is not designed to take load during impact, relying on the load bearing capabilities of the retention system may be a concern; the ability for a retention system to bear load may not be as reliable in minimizing linear head accelerations. In select high-speed video, the retention system could be observed separating from the helmet liner. However, all simulated impacts remained under 300 g, the threshold associated with skull fracture. Even the highest recorded linear accelerations in any impact scenario were under 200 g. As long as the helmet is sufficiently covering the impact location, skull fracture is not an increased concern with poor helmet fit.

5.4.2   Diffuse Injury

Considering diffuse injury and angular velocity, CSDM, and MPS, the likelihood of brain injury was not increased as a result of poor helmet fit in head-first impacts. However, the same trends were not observed in torso-first impacts. For torso first-impacts, a oversized and forward fit may reduce the likelihood of brain injury while a backward fit may increase the likelihood. It should be kept in mind that these results are representative for presented impact scenarios which only consisted of forehead

impacts in this work.

For head first impacts, the likelihood of brain injury was not significantly different in different fit scenarios. Angular velocity, CSDM, and MPS, all showed small changes between between different fit scenarios. In only a specific impact and backward fit scenario, CSDM and MPS was statistically significant with the case of an oversized helmet in an angled anvil impact, but this result was not practically significant due to the small changes in injury risk.

For torso-first impacts, CSDM results showed potential changes in brain injury likelihood for a poor helmet fit. Both an oversized and forward fit scenario showed decreased brain injury risk at low impact velocities while a backward fit showed increased brain injury risk at high impact velocities. Similar trends were observed in angular kinematics and MPS, but only CSDM results were significant. Most of the peak angular velocities in the experiments ranged from 15 - 30 rad/s, with a backward fit scenario reaching up to 41.24 rad/s. In Margulies work, an angular velocity threshold of 46.5 rad/s was associated with moderate to severe diffuse axonal injury [60]. Because a backward fit scenario nearly reaches magnitudes associated with brain injury, the potential increases in brain injury likelihood is noteworthy. With the brain finite element modeling in this backward fit scenario, the maximum MPS in this work could be found to correspond with a 9.4% risk of diffuse axonal injury [29].

A potential explanation for the differences in angular kinematics between head-first and torso-first may be due to the different contact mechanisms during impact. In the torso-first impacts, neck flexion allowed the head and neck to pivot around the torso. This neck movement allows the angle of the head to change during impact. As a result, the contact point on the helmet was variable between fit scenarios. In the backward fit scenarios, for instance, the impact was able to contact the helmet brim as opposed to the main body of the helmet. This would allow the impact force of the head

impact to act in a more tangential direction and introduce more angular movement. In the oversized and forward fits, a greater portion of the forehead was protected by the helmet. The sufficient coverage of the oversized and forward fit helmets could then allow the impact to occur consistently on the body of the helmet as opposed to the brim. The results obtained from tracking helmet movement could be interpreted to show a consistent theme with variations in contact mechanics during impact. The normal and backward fits, the scenarios most susceptible to impacts to the helmet brim, both showed the greatest amount of helmet displacement. The backward fit, in particular, was most susceptible and also showed the most head-helmet displacement.

5.4.3 Head Exposure

Considering max head-helmet displacements, d_{max}, a backward fit scenario showed significant amounts of head exposure. The excessive exposure is indicated by the greatest amounts of peak head-helmet displacements (d_{max}). By looking at relative head-helmet displacements, Δd, helmet movement did not significantly change between different scenarios.

A backward fit scenario seemed to lead to the greatest amount of head exposure, which is concerning because exposing the head could lead to inadequate head protection in subsequent impacts. The excess exposure of the head was largely due to the increased forehead exposure prior to impact due to poor helmet fit. In contrast, the oversized and forehead fit scenarios already have the helmet expose less of the forehead even before an impact. As a result, forehead exposure is already reduced.

Helmet movement appeared to be consistent between different fit scenarios in head first impacts, but not in one torso first impact scenario. The increased helmet movement in torso-first impacts can be similarly attributed to the different contact mechanics due to neck flexion, allowing more of the helmet brim to be contacted. In the extreme cases, the excessive displacement in the normal and backward fit

scenarios was enough to expose the forehead after the initial impact. Exposure of the bare head should be of utmost concern because any subsequent impacts would then be able to directly contact the head without protection.

5.4.4 Neck Injury

In terms of neck injury, the different fit scenarios showed similar levels of Nij. As such, it is concluded that different fit scenarios do not increase the risk of neck injury. With neck injuries uncommon in cycling [9], it is unlikely that helmet fit has a significant effect on increasing neck injury likelihood.

5.4.5 Fit Forces for Quantifying Fit

Fit forces were intended to distinguish the fit scenarios to ideally predict trends in a helmet's performance. However, the biomechanical metrics associated with injury risk show that different fit scenarios perform differently in different impact scenarios. A particular fit scenario did not pose the same injury risk across all impact scenarios. Conclusions could not be made that a loose fitting helmet with low fit forces would be more susceptible to helmet movement. As such, the measurement of fit forces was not particularly valuable for predicting helmet performance.

5.4.6 Overall Trends

From the presented results, it appears that helmet fit did not have an effect on focal head injury; peak g was unchanged in many cases, and in cases where it was changed the risk of focal injury was small. Considering diffuse injury, fit did not have a consistent effect on injury risk. In the small subset of results that did indicate a significant effect (based on p-value), the percentage change in injury risk was small. Specific to neck injury, fit did not alter injury risk. The simple interpretation of these findings is that, if the helmet is retained on the head, then it is effective at protecting

the wearer. Fit did seem to effect the amount of the head that was exposed by the end of the impact event. This result could be viewed as problematic because more head exposure results in unprotected regions which could be injured in subsequent impacts.

5.4.7 Equipment Limitations

As with all biomechanical work based on ATDs, there are limitations in the presented methods. Unlike real world impacts, parameters such as impact speed, impact location on the helmet, and impact surfaces are controlled. Therefore, the work presented will not capture the variability of these parameters from cyclist to cyclist and from incident to incident leading to head impact. The effort was made to capture a variety of impact scenarios by varying impact speed, a tangential velocity component, and whether the head or torso was impacted first. However, only forehead impacts were performed. Other impact locations are also common and important to investigate.

The Hybrid III was developed for automotive crash testing, as opposed to helmet research. Unlike a National Operating Committee on Standards for Athletic Equipment (NOCSAE) headform, it was not designed to wear a helmet [11]. In contrast, the NOCSAE headform was designed with size and shape specifications based on cadaver heads for an average adult football player and some consider it to more accurately approximate head anthropometry. Because helmet fit is dependent on head geometry, the Hybrid III could be criticized for certain shortcomings when used with a helmet. In particular, the headform has notable geometrical differences to the NOCSAE head in the base of the skull, cheeks, jaw, and chin [37, 36]. In the presented experiments, however, the open face bicycle helmets have minimal interaction between these anatomical features on the headform. Only the chinstrap comes into contact with these features. If helmets of different style, such as football helmets or full face bicycle helmets, were used, using the Hybrid III head may have more

pronounced differences as a result of geometry dissimilarities.

Related to the headform head, the corresponding Hybrid III neck has been criticized for its greater stiffness compared to a human neck. Some hypothesize that the lack of realistic stiffness can contribute to head motions that differ from those of a real human suffering head impact [39]. These effects would be considerably more significant in the torso-first impacts because the trajectory and kinematics of the head are dependent on the neck. For a torso-first impact, an overly stiff neck could attenuate the head's motion after the torso contact and unrealistically slow the head's impact velocity at head contact. A human head could experience greater angular accelerations, corresponding to a higher likelihood of brain injury. With limited existing literature investigating torso-first impacts, the biofidelity of the kinematic traces are difficult to validate with real-world cyclists impacts. However, head angular acceleration from the torso traces are comparable to similar combined loading scenarios performed by Smith et al [53]. Again, the trends in angular acceleration and neck load in different fit scenarios should be emphasized, rather than reported absolute magnitudes.

Another limitation of using the headform in studying helmet fit is the dissimilarity of the headform vinyl skin with that of a human scalp. Many differences exist between the Hybrid III headform and a human head, such as variations in hair, oil, and moisture. Accurately accommodating all these variables would be difficult. Although efforts in creating an artificial scalp for helmet research have been pursued [38], validations of head helmet interaction between artificial and human scalps have been minimal. In order to maintain repeatability for other researchers, no modifications to the scalp were made. Since it is generally accepted that the headform skin exhibits a higher coefficient of friction than a human scalp, helmet movement could be minimized. This lack of movement could misleadingly suggest sufficient helmet retention. With varying dependence on head-helmet friction in different fit scenarios,

the effect of the headform vinyl skin could also be more or less pronounced. For instance, a normal fit scenario may retain a helmet due to head shape while a forward fit may retain a helmet due to the increased head-helmet friction of the vinyl skin. However, the helmet displacements are dependent on the headform scalp in this study. Accordingly, findings are based on changes and trends, rather than absolute displacements.

Limitations in fit force sensor spatial resolution, discussed in Chapter 3, also limited the ability to better capture fit forces. However, it was also discussed that determining contact area may be of importance as well. With the interpretation that different fit scenarios may perform differently due to different contact areas, knowing the contact area could be particularly telling.

With the presented method in measuring head-helmet displacement, the metric is able to characterize the amount of forehead exposure. However, this metric does not characterize head exposure elsewhere from the forehead, and is most appropriate for quantifying helmet movement forehead impacts. Because only forehead impacts were performed, this was not a problem. However, simulation of other impact locations would result in different helmet movement. The metric should be modified for different impact locations in order to capture rotation about different axes.

Chapter 6

Conclusion

6.1   Contributions

In this thesis, the primary goal of the work was to investigate the effect of helmet fit on injury likelihood with the intention of answering the question of whether or not improper helmet use would change an individual's risk of head and neck injury. In investigating this research question, an ATD headform impact testing set-up was used to simulate different fit conditions under different impact scenarios. Two new tools were first created to more comprehensively perform the study.

With an existing ATD headform impact testing equipment, head and neck injury likelihood could be quantified in terms of head kinematics and neck kinetics. To better investigate helmet fit, new methods were developed to quantify helmet fit and track head exposure during impact. In quantifying helmet fit, a fit force sensor was designed using optical FBG sensors. A sensor array was then successfully implemented to measure fit forces of different fit scenarios. The capabilities of this methodology were investigated. To measure helmet movement, a novel method using dual high speed cameras was developed. This method proved to produce repeatable results and provided insight into helmet movement during impact. The newly developed method presents the opportunity to understand helmet movement that is not investigated in

other work, and can be applied in studies beyond helmet fit.

With these methods, new findings on the effect of helmet fit on injury likelihood were investigated. Experiments were performed that include more fit and impact scenarios than previous studies. In the context of studying helmet fit, this work is the first to look at either angled anvil or torso-first impact scenarios. It is also the first to look at neck kinetics and head-helmet displacements resulting from different fit scenarios. Compared to similar work investigating helmet fit, drops with similar fit and impact conditions as other studies proved to be consistent.

Overall, the results of the study suggest that poor helmet fit does not increase most injury metrics:

- Risk of focal injury does not increase with poor helmet fit, as suggested by peak linear acceleration.

- Risk of diffuse injury does not increase, except in the select case of a torso-impact with a backward helmet fit. This was shown with angular kinematics and brain strains.

- Risk of neck injury does not increase with poor helmet fit, as shown by unchanged Nij values.

- Head exposure may increase with a backward fit helmet, exposing the head to risk in subsequent impacts. This was shown by tracking helmet movement during an impact and measuring "head-helmet displacement".

The results suggest that as long as a helmet sufficiently covers the head, risks of injury does not increase. However, poor helmet fit may allow the helmet to be displaced and expose the head in subsequent impacts. The ability for a helmet to protect the head may then place increased emphasis on helmet retention systems. The results in this thesis document trends in biomechanical measures from a laboratory

study with several limitations. These results should not be construed to indicate deficiency in the design of the helmets used.

6.2 Future Work and Recommendations

In understanding the effect of helmet fit on injury likelihood, the current work may be continued. In particular, different helmet fit scenarios and impact scenarios could be investigated. For helmet fit, only a forward/backward position and oversized helmet scenarios were found. However, other variables can also be used to characterized proper helmet use. For instance, other fit scenarios could include an undersized helmet exhibiting a tighter fit. Different levels of tightness in retention system, both in the chin strap and adjustable ratchet system, could be be investigated. Comparisons between different helmet types could also be pursued, whether the difference is in helmet type design or different activity. With all these different fit scenarios, the same methodology presented could be used to fully investigate head exposure, head injury, and neck injury. In terms of impact scenarios, all the impacts performed in this work were limited to forehead impacts. Because other impacts to other locations on the head are also common, varying impact location should be the one of the first variables to study in further investigating helmet fit in different impact scenarios. However, some modifications to the methods should be made, such as expanding on the capabilities for head-helmet displacement.

Another valuable adjustment that could be included in the experimental set up is a more realistic headform scalp. Helmet fit relies on coupling between the head and helmet, which may be over-represented by the Hybrid III head's increased coefficient of friction. This increased friction could cause better coupling between the head and helmet, and cause less helmet movement. As such, the helmet may better cover the head during the impact or may even transfer more rotational movement to the head.

Overall, the Hybrid III may have downplayed the possible sliding between a head and helmet. Although an realistic scalp would be valuable, no such scalp currently exists. Furthermore, the variations in human scalp from person to person would further add complexity in creating a model that is representative.

To further expand on the understanding of helmet fit, the characterization of different fit scenarios could also be explored. In particular, quantifying contact area between head and helmets before and during impact could be particularly valuable. Because different fit scenarios can result in different levels of injury risk, being able to better differentiate different fit scenarios could help understand factors affecting head injury risk.

To better reinforce any similar work regarding helmet fit, further work could validate that the fit scenarios are representative of actual use. For instance, scenarios could be recreated based on volunteer feedback. In this thesis, the ratchet retention system was tightened to a consistent level of tightness, subjective to the researcher. However, a tightness could be chosen based on loads experienced by an individual. In Jadischke's fitment study, football helmets were inflated corresponding to pressures experienced by volunteers wearing helmets. A similar technique could be applied in this work with bicycle helmets by using helmet sizes and levels of tightness corresponding to volunteers. By measuring the fit forces of a ratchet on volunteers, a helmet could be tightened and adjusted accordingly. This added step could support decisions in fit scenarios, as well as show whether or not an individual's perceived proper fit corresponds to the best helmet performance.

The newly developed method for characterizing helmet movement could also be extended in studies beyond helmet fit. In any scenario where helmet stability, retention, or head exposure is of interest, these methods become valuable in providing better understanding of head-helmet interaction.

REFERENCES

[1] Jean A Langlois, Wesley Rutland-Brown, and Marlena M Wald. The epidemiology and impact of traumatic brain injury: a brief overview. *The Journal of head trauma rehabilitation*, 21(5):375–378, 2006.

[2] Christopher A Taylor. Traumatic brain injury–related emergency department visits, hospitalizations, and deathsunited states, 2007 and 2013. *MMWR. Surveillance Summaries*, 66, 2017.

[3] Diane C Thompson, Frederick P Rivara, and Robert S Thompson. Effectiveness of bicycle safety helmets in preventing head injuries: a case-control study. *Jama*, 276(24):1968–1973, 1996.

[4] Peter A Cripton, Daniel M Dressler, Cameron A Stuart, Christopher R Dennison, and Darrin Richards. Bicycle helmets are highly effective at preventing head injury during head impact: Head-form accelerations and injury criteria for helmeted and unhelmeted impacts. *Accident Analysis & Prevention*, 70:1–7, 2014.

[5] Gregory W Parkinson and Kelly E Hike. Bicycle helmet assessment during well visits reveals severe shortcomings in condition and fit. *Pediatrics*, 112(2):320–323, 2003.

[6] Frederick P Rivara, Susan J Astley, Sterling K Clarren, Diane C Thompson, and Robert S Thompson. Fit of bicycle safety helmets and risk of head injuries in children. *Injury Prevention*, 5(3):194–197, 1999.

[7] RS Lee, Brent Edward Hagel, M Karkhaneh, and BH Rowe. A systematic review of correct bicycle helmet use: how varying definitions and study quality influence the results. *Injury prevention*, 15(2):125–131, 2009.

[8] Jake Olivier and Prudence Creighton. Bicycle injuries and helmet use: a systematic review and meta-analysis. *International journal of epidemiology*, 46(1):278–292, 2017.

[9] Frederick P Rivara, Diane C Thompson, and Robert S Thompson. Epidemiology of bicycle injuries and risk factors for serious injury. *Injury prevention*, 21(1):47–51, 2015.

[10] CPSC - Safety Standard for Bicycle Helmets; Final Rule, March 1998.

[11] Standard Test Method and Equipment used in Evaluating the Performance Characteristics of Protective Headgear/Equipment NOCSAE Doc (ND) 001- 11m12, 2012.

[12] Ron Jadischke. Football helmet fitment and its effect on helmet performance. Master's thesis, Wayne State University, 2012.

[13] Thierry Ellena, Aleksandar Subic, Helmy Mustafa, and Toh Yen Pang. The helmet fit index–an intelligent tool for fit assessment and design customisation. *Applied ergonomics*, 55:194–207, 2016.

[14] Thomas Gennarelli. Head injury mechanisms. In Joseph S Torg, editor, *Athletic Injuries to the Head, Neck, and Face.*, chapter 18, pages 232–240. Mosby-Year Book, Inc, St. Louis, MO, 1991.

[15] Ian D Civil and C William Schwab. The abbreviated injury scale, 1985 revision: a condensed chart for clinical use. *Journal of Trauma and Acute Care Surgery*, 28(1):87–90, 1988.

[16] Kai-Uwe Schmitt, Peter F Niederer, Duane S Cronin, Markus H Muser, and Felix Walz. *Trauma biomechanics: an introduction to injury biomechanics.* Springer Science & Business Media, 2014.

[17] Philip Yarnell and Ayub K Ommaya. Experimental cerebral concussion in the rhesus monkey. *Bulletin of the New York Academy of Medicine*, 45(1):39, 1969.

[18] Thomas A Gennarelli, LE Thibault, and Ayub K Ommaya. Pathophysiologic responses to rotational and translational accelerations of the head. Technical report, SAE Technical Paper, 1972.

[19] Peter Cummings, Frederick P Rivara, Diane C Thompson, and Robert S Thompson. Misconceptions regarding case-control studies of bicycle helmets and head injury. *Accident Analysis & Prevention*, 38(4):636–643, 2006.

[20] William J Curnow. Bicycle helmets and brain injury. *Accident Analysis & Prevention*, 39(3):433–436, 2007.

[21] Voigt R. Hodgson. Impact standards for protective equipment. In Joseph S Torg, editor, *Athletic Injuries to the Head, Neck, and Face.*, chapter 18, pages 28–43. Mosby-Year Book, Inc, St. Louis, MO, 1991.

[22] Elisha S Gurdjian, VL Roberts, and L Murray Thomas. Tolerance curves of acceleration and intracranial pressure and protective index in experimental head injury. *Journal of Trauma and Acute Care Surgery*, 6(5):600–604, 1966.

[23] Rolf Eppinger, Emily Sun, Faris Bandak, Mark Haffner, Nopporn Khaewpong, Matt Maltese, Shashi Kuppa, Thuvan Nguyen, Erik Takhounts, Rabih Tannous,

et al. Development of improved injury criteria for the assessment of advanced automotive restraint systems–ii. *National Highway Traffic Safety Administration*, pages 1–70, 1999.

[24] Steven P Broglio, Jacob J Sosnoff, SungHoon Shin, Xuming He, Christopher Alcaraz, and Jerrad Zimmerman. Head impacts during high school football: a biomechanical assessment. *Journal of athletic training*, 44(4):342–349, 2009.

[25] Erik G Takhounts, Matthew J Craig, Kevin Moorhouse, Joe McFadden, and Vikas Hasija. Development of brain injury criteria (bric). *STAPP car crash journal*, 57:243, 2013.

[26] James A. Newman. A generalised model for brain injury threshold (GAMBIT). In *International IRCOBI Conference on the Biomechanics of Impact, International Research Council on the Biomechanics of Impact, Bron, France*, pages 17–36, 1986.

[27] James A Newman, Nicholas Shewchenko, and Eric Welbourne. A proposed new biomechanical head injury assessment function-the maximum power index. *STAPP car crash journal*, 44:215–247, 2000.

[28] Erik G Takhounts, Rolf H Eppinger, J Quinn Campbell, Rabih E Tannous, et al. On the development of the simon finite element head model. *STAPP car crash journal*, 47:107, 2003.

[29] Erik G Takhounts, Stephen A Ridella, Vikas Hasija, Rabih E Tannous, J Quinn Campbell, Dan Malone, Kerry Danelson, Joel Stitzel, Steve Rowson, and Stefan Duma. Investigation of traumatic brain injuries using the next generation of simulated injury monitor (simon) finite element head model. *STAPP car crash journal*, 52:1, 2008.

[30] Christopher R Dennison, Erin M Macri, and Peter A Cripton. Mechanisms of cervical spine injury in rugby union: is it premature to abandon hyperflexion as the main mechanism underpinning injury? *British Journal of Sports Medicine*, 46(8):545–549, 2012.

[31] Amy Saari, Christopher R Dennison, Qingan Zhu, Timothy S Nelson, Philip Morley, Thomas R Oxland, Peter A Cripton, and Eyal Itshayek. Compressive follower load influences cervical spine kinematics and kinetics during simulated head-first impact in an in vitro model. *Journal of biomechanical engineering*, 135(11):111003, 2013.

[32] Albert I King. Fundamentals of impact biomechanics: part i-biomechanics of the head, neck, and thorax. *Annual review of biomedical engineering*, 2(1):55–81, 2000.

[33] Michael Kleinberger, Emily Sun, Rolf Eppinger, Shashi Kuppa, and Roger Saul. Development of improved injury criteria for the assessment of advanced automotive restraint systems. *NHTSA Docket*, (1998-4405):9, 1998.

[34] CA Morehouse. The ASTM F 1045-07 standard performance specification for ice hockey helmets. In *Safety in Ice Hockey*. ASTM International, 2007.

[35] Canadian Standards Association et al. CAN/CSA Z262. 1-09. *Ice Hockey Helmets. National Standard of Canada*, 2009.

[36] Bryan R Cobb, Anna MacAlister, Tyler J Young, Andrew R Kemper, Steven Rowson, and Stefan M Duma. Quantitative comparison of Hybrid III and National Operating Committee on Standards for Athletic Equipment headform shape characteristics and implications on football helmet fit. *Proceedings of the Institution of Mechanical Engineers, Part P: Journal of Sports Engineering and Technology*, 229(1):39–46, 2015.

[37] Bryan R Cobb, Abigail M Zadnik, and Steven Rowson. Comparative analysis of helmeted impact response of Hybrid III and national operating committee on standards for athletic equipment headforms. *Proceedings of the Institution of Mechanical Engineers, Part P: Journal of Sports Engineering and Technology*, 230(1):50–60, 2016.

[38] Magnus Aare and Peter Halldin. A new laboratory rig for evaluating helmets subject to oblique impacts. *Traffic injury prevention*, 4(3):240–248, 2003.

[39] M De Jager, A Sauren, J Thunnissen, and J Wismans. A global and a detailed mathematical model for head-neck dynamics. Technical report, SAE Technical Paper, 1996.

[40] James A Newman, Marc C Beusenberg, Nicholas Shewchenko, Chris Withnall, and E Fournier. Verification of biomechanical methods employed in a comprehensive study of mild traumatic brain injury and the effectiveness of american football helmets. *Journal of biomechanics*, 38(7):1469–1481, 2005.

[41] Federal Motor Vehicle Safety Standard. Office of vehicle safety compliance laboratory test procedure no. 218; motorcycle helmets. *Washington, DC: NHTSA, Department of Transportation*, 2011.

[42] Li-Tung Chang, Chih-Han Chang, and Guan-Liang Chang. Fit effect of motorcycle helmet. *JSME International Journal Series A Solid Mechanics and Material Engineering*, 44(1):185–192, 2001.

[43] Andrew S McIntosh, Adrian Lai, and Edgar Schilter. Bicycle helmets: head impact dynamics in helmeted and unhelmeted oblique impact tests. *Traffic injury prevention*, 14(5):501–508, 2013.

[44] Corina Klug, Florian Feist, and Ernst Tomasch. Testing of bicycle helmets for preadolescents. *Int. Res. Council Biomech. Inj.(IRCOBI)*, pages 136–155, 2015.

[45] Robert C Butz and Christopher R Dennison. In-fiber bragg grating impact force transducer for studying head–helmet mechanical interaction in head impact. *Journal of Lightwave Technology*, 33(13):2831–2838, 2015.

[46] Robert C Butz, Brooklynn M Knowles, James A Newman, and Christopher R Dennison. Effects of external helmet accessories on biomechanical measures of head injury risk: An atd study using the Hybrid III headform. *Journal of biomechanics*, 48(14):3816–3824, 2015.

[47] Robert Calyn Butz. An impact force transducer for anthropomorphic test dummy headforms: Application to study effects of external helmet accessories on biomechanical measures of head injury risk. Master's thesis, University of Alberta, 2015.

[48] Christopher Raymond Stuart Dennison. *Development and application of in-fibre Bragg grating based biomedical pressure sensors*. PhD thesis, University of Victoria, 2008.

[49] Norman R Miller, Robert Shapiro, and Thomas M McLaughlin. A technique for obtaining spatial kinematic parameters of segments of biomechanical systems from cinematographic data. *Journal of Biomechanics*, 13(7):535543–541547, 1980.

[50] K Somani Arun, Thomas S Huang, and Steven D Blostein. Least-squares fitting of two 3-d point sets. *IEEE Transactions on pattern analysis and machine intelligence*, (5):698–700, 1987.

[51] Henry Yu, Brooklynn M Knowles, and Christopher R Dennison. A test bed to examine helmet fit and retention and biomechanical measures of head and neck injury in simulated impact. *Journal of Visualized Experiments*, 2017 (In Press).

[52] Society of Automotive Engineers. SAE J211 Instrumentation for Impact Test - Part 1: Electronic Instrumentation, 2007.

[53] Terry A Smith, P David Halstead, Elizabeth McCalley, Scott A Kebschull, Scott Halstead, and James Killeffer. Angular head motion with and without head contact: implications for brain injury. *Sports Engineering*, 18(3):165–175, 2015.

[54] AJ Padgaonkar, KW Krieger, and AI King. Measurement of angular acceleration of a rigid body using linear accelerometers. *Journal of Applied Mechanics*, 42(3):552–556, 1975.

[55] Harold J Mertz, Annette L Irwin, and Priya Prasad. Biomechanical and scaling bases for frontal and side impact injury assessment reference values. *Stapp car crash journal*, 47:155, 2003.

[56] Brooklynn M Knowles, Henry Yu, and Christopher R Dennison. Accuracy of a wearable sensor for measures of head kinematics and calculation of brain tissue strain. *Journal of Applied Biomechanics*, 33(1):2–11, 2017.

[57] Brooklynn M. Knowles, Samantha R. MacGillivray, James A. Newman, and Christopher R. Dennison. Influence of rapidly successive head impacts on brain strain in the vicinity of bridging veins. *Journal of Biomechanics*, 59:59 – 70, 2017.

[58] Narayan Yoganandan, Mark Haffner, Dennis J Maiman, Hunter Nichols, Frank A Pintar, Jeffrey Jentzen, Steven S Weinshel, Sanford J Larson, and Anthony

Sances. Epidemiology and injury biomechanics of motor vehicle related trauma to the human spine. Technical report, SAE Technical Paper, 1989.

[59] Johan Ivarsson, David C Viano, P Lovsund, and Y Parnaik. Head kinematics in mini-sled tests of foam padding: Relevance of linear responses from free motion headform (FMH) testing to head angular responses. *Journal of biomechanical engineering*, 125(4):523–532, 2003.

[60] Susan Sheps Margulies and Lawrence E Thibault. A proposed tolerance criterion for diffuse axonal injury in man. *Journal of biomechanics*, 25(8):917–923, 1992.

Appendix A

Metric Calculation

This Appendix outlines the rationale and use of helmet fit metrics and different metrics used in this thesis. These metrics include quantification of fit, injury metrics, and head-helmet displacement characterization.

A.1 Helmet Fit Forces

Global fit force aims to communicate the overall tightness exhibited by a helmet onto a head. The global fit force is an average from all the force measurements from each sensor. A high value represents a tight fit.

$$GlobalFitForce = \frac{F_1 + F_2 + ... + F_N}{N} \tag{A.1}$$

where

$$F_i \quad = \quad \text{Fit Force Measured from a Single Sensor [N]}$$

$$N \quad = \quad \text{Number of Sensors}$$

Global fit force variation aims to communicate the variation in tightness exhibited

by a helmet onto a head. The global fit force variation is equivalent to the standard deviation calculated from the force measurements from each sensor. A higher value represents uneven tightness.

$$GlobalFitForceVariation = \sqrt{\frac{\sum_{i=1}^{N}(F_i - GlobalFitForce)^2}{n-1}} \qquad \text{(A.2)}$$

A.2 Head Kinematic Metrics

Linear acceleration (Figure A.1) can be used to indicate the severity of a head impact related to focal injury and is often measured in g (1 g $= 9.81\text{m/s}^2$). Resultant linear acceleration is the norm of the x, y, and z components. Resultant Peak g is the maximum value of the resultant at any point in the impact.
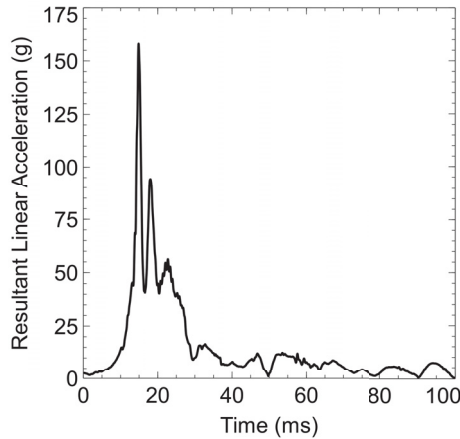
Figure A.1: Resultant Linear Acceleration

Angular kinematics can be used to indicate the severity of a head impact related to diffuse injury, and can be characterized as angular acceleration (Figure A.2) or angular velocity (Figure A.3). Angular velocity can be found through integration of angular acceleration. Resultant peak angular acceleration, α, and peak angular velocity, ω, can be found as the maximum value of their resultants at any point in impact. Change in angular velocity, $\Delta\omega$ can also be determined by taking the

difference between the maximum and minimum angular velocity.
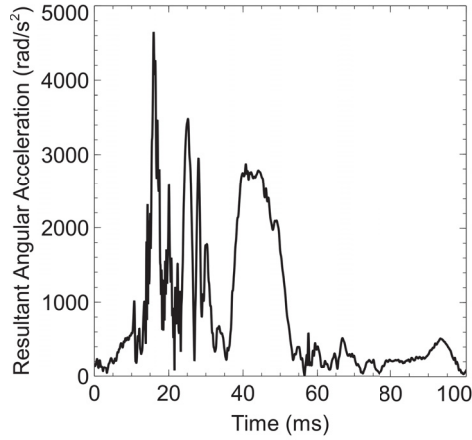
Figure A.2: Resultant Angular Acceleration
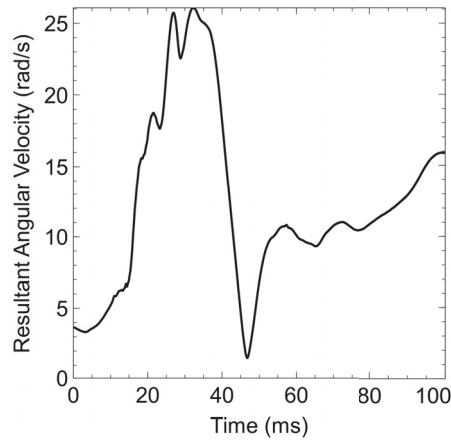
Figure A.3: Resultant Angular Velocity

A.3   Brain Finite Element Model Metrics (CSDM and MPS)

Evaluating likelihood of diffuse injury may also include the use of brain finite element models. By using head kinematics as input for the model, strains in the brain may be determined. More strain in the brain would then correlate with more damage in brain tissue, which presumably results in more brain injury. For this thesis, the Simulated Injury Monitor (SIMon) was used to determine cumulative strain damage measure

(CSDM) and maximum principle strain (MPS). During an impact, each CSDM and MPS reach a limit (Figures A.4 and A.5). The maximum that each of these measures reaches is reported as the CSDM and MPS value. CSDM represents the volume fraction of the brain reaching a certain strain threshold. In this thesis, CSDM 15, the volume fraction of the brain reaching 15% strain, is reported.
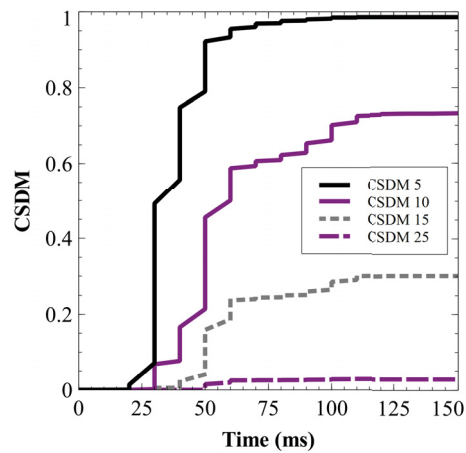
Figure A.4: Cumulative Strain Damage Measure
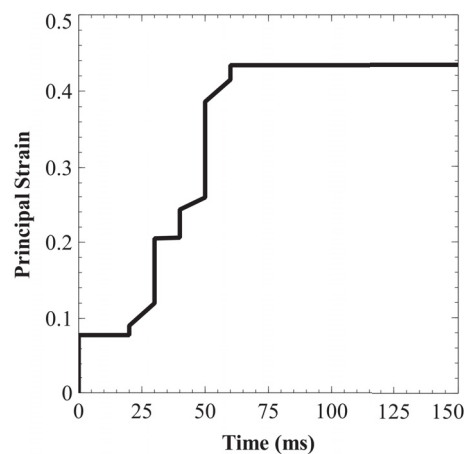
Figure A.5: Maximum Principal Strain

A.4 Neck Injury

The severity of neck injury can be characterized using the Neck Injury Criterion, Nij, which combines axial and bending loading of the neck (Figure A.6). This criterion also takes into consideration the critical axial and bending limits for different loading conditions and geometries. For instance, different limits exist for flexion and extension. For use with a Hybrid III neck, there also exists a specific set of critical limits. Nij can be calculated with the following equation.

$$N_{ij} = \frac{F_z}{F_{int}} + \frac{M_y}{M_{int}} \tag{A.3}$$

where

$$
\begin{aligned}
F_z &= \text{Axial Load [N]} \\
F_{int} &= \text{Critical Axial Load [N]} \\
M_y &= \text{Flexion/Extension Bending Moment [N.m]} \\
M_{int} &= \text{Critical Flexion/Extension Bending Moment [N.m]}
\end{aligned}
$$

In this thesis, Nij is reported as the maximum Nij value reached during an impact.
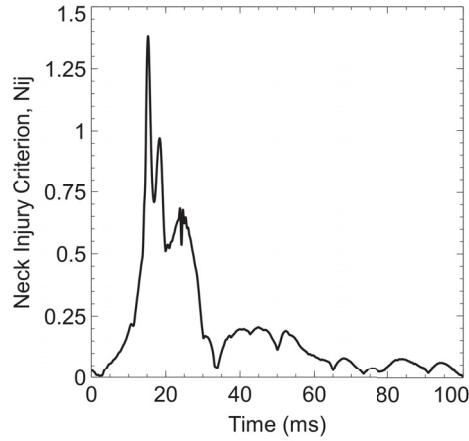
Figure A.6: Nij, Neck Injury Criterion

A.5 Head-Helmet Displacement

The methods used for determining head-helmet displacement are developed in Chapter 4, with the experimental equipment and procedure detailed in Section 4.5. Two metrics can be derived from absolute head-helmet displacement during an impact (Figure A.7). Peak Head-Helmet Displacement, d_{max}, is used to characterize the amount of head exposure while relative change in displacement, Δd, is used to character helmet movement. d_{max} can be found by simply taking the maximum displacement during an impact, while Δd is found by taking difference between the starting and maximum displacement.
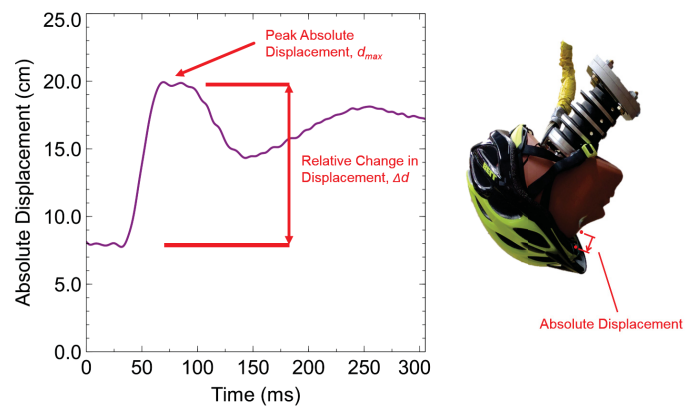
Figure A.7: Head Helmet Displacement

Relative change in displacement is also indicated. The vector for absolute displacement is also shown on the right.